1966

Microwave Hall mobilities of holes in germanium

Bou-loong Ho
Iowa State University

66-6983

HO, Bou-loong, 1930-

MICROWAVE HALL MOBILITIES OF HOLES IN GERMANIUM.

Iowa State University of Science and Technology
Ph.D., 1966
Engineering, electrical

MICROWAVE HALL MOBILITIES OF HOLES IN GERMANIUM

by

Bou-loong Ho

A Dissertation Submitted to the

Graduate Faculty in Partial Fulfillment of

The Requirements for the Degree of

DOCTOR OF PHILOSOPHY

Major Subject: Electrical Engineering

Approved:

Signature was redacted for privacy.

In Charge of Major Work

Signature was redacted for privacy.

Head of Major Department

Signature was redacted for privacy.

Dean of Graduate College

Iowa State University
Of Science and Technology
Ames, Iowa

1966

TABLE OF CONTENTS

		Page
	ABSTRACT	v
I.	INTRODUCTION	1
	A. Hall and Faraday Effects	1
	B. Previous Work on Microwave Hall Effect Measurement	5
	C. Band Structure of p-type Germanium (13)	5
	D. Mobility of Holes	7
	E. Purpose of Investigation	10
II.	EXPERIMENTAL PROCEDURE	11
	A. Microwave Measurement	11
	1. Principle of microwave measurement	11
	2. Microwave cavity system	14
	3. Cryostat system and temperature control	18
	4. Sample preparation	20
	5. Microwave measurement procedures	21
	B. d.c. Measurement	24
III.	EXPERIMENTAL RESULTS	26
	A. Field Dependence Measurement	26
	B. Temperature Dependence Measurement	28
IV.	DISCUSSION	35
	A. Charge Carrier Inertia	35
	B. Mixed Scattering by Lattice Vibrations and Ionized Impurities	42
	C. Hole Contribution to the Dielectric Constant	43
	D. Conclusions	44
	E. Future Work	45
V.	LITERATURE CITED	47
VI.	ACKNOWLEDGMENTS	52
VII.	APPENDIX	53

LIST OF FIGURES

		Page
Fig. 1.	Principle of microwave Hall mobility measurement	12
Fig. 2.	Cavity construction for low temperature measurement	16
Fig. 3.	Cryostat	19
Fig. 4.	Schematic diagram of microwave circuit	22
Fig. 5.	Magnetic field dependence of $\sqrt{\frac{P_2}{P_1}}$ for p-type germanium single crystals	27
Fig. 6.	Hall mobility of p-type germanium single crystals vs. temperature	31
Fig. 7.	$\frac{(u_H)dc - (u_H)mv}{(u_H)_{dc}}$ vs. temperature	32
Fig. 8.	Resistivity of p-type germanium single crystals vs. reciprocal of temperature	33
Fig. 9.	Real and imaginary parts of $\frac{\sigma(\omega)}{\sigma(0)}$ for single-valley model and nondegenerate statistics	38
Fig. 10.	Real and imaginary parts of $\frac{\theta(\omega)}{\theta(0)}$ for single-valley model and nondegenerate statistics	39
Fig. 11.	$\frac{u_H(\omega)}{u_H(0)}$ for single-valley model and nondegenerate statistics	41

LIST OF TABLES

		Page
Table 1.	d.c. electrical measurement of p-type germanium (439HGP)	53
Table 2.	d.c. electrical measurement of p-type germanium (GP1)	55
Table 3.	d.c. electrical measurement of p-type germanium (439GP)	56
Table 4.	Magnetic field dependence of $\sqrt{\frac{P_2}{P_1}}$ for p-type germanium single crystals	58
Table 5.	Microwave Hall mobility of p-type germanium (439HGP) at low temperature	59
Table 6.	Microwave Hall mobility of p-type germanium (GP1) at low temperature	60
Table 7.	Microwave Hall mobility of p-type germanium (439GP) at low temperature	61
Table 8.	$\frac{(u_H)_{dc} - (u_H)_{mv}}{(u_H)_{dc}}$ vs. temperature	62

ABSTRACT

Hall mobilities of three p-type germanium crystals were measured at microwave frequencies of 9.5 G Hz from room temperature to near liquid helium temperatures by means of a newly designed bimodal rectangular cavity. The microwave Hall mobilities were compared with the corresponding d.c. Hall mobilities. As the temperature was decreased, the microwave Hall mobility began to deviate from the d.c. Hall mobility at about 200°K for each of the less pure samples 439GP and GP1, but not until 150°K for the purest sample 439HGP. The difference between the microwave and d.c. Hall mobilities at low temperatures was greater in the order 439GP > GP1 > 439HGP, whereas the purity of the samples followed the opposite order 439HGP > GP1 > 439GP. The difference between the microwave and d.c. Hall mobilities can be explained in terms of a high frequency inertial effect in which the relaxation time depends upon scattering of the holes by impurities as well as by phonons. This inertial effect accounts for the experimental results: one, at low temperatures, the microwave Hall mobility was always lower than the corresponding d.c. Hall mobility; and two, an increase in impurity scattering always increased the difference between the microwave and d.c. mobilities of the holes.

I. INTRODUCTION

A. Hall and Faraday Effects

When we solve the Boltzmann equation (1)

$$\frac{\partial f}{\partial t} + e\,[\vec{E} + \vec{V} \times \vec{B}] \cdot \frac{1}{\hbar} \vec{\nabla}_k f + \vec{V} \cdot \vec{\nabla}_r f = \left[\frac{\partial f}{\partial t}\right]_c \qquad (1.1)$$

for the time-independent fields, in the limit of low magnetic fields, a general expression for the current density to the first order in magnetic induction can be obtained in tensor notation (2)

$$j_\eta = \sigma_\eta E_\eta + \theta_{\eta\xi\rho} E_\xi B_\rho, \qquad (1.2)$$

where the subscripts η, ξ and ρ run over cartesian coordinates and

$\vec{V}$ = velocity vector,

f = the distribution function of the carriers,

$\vec{B}$ = applied static magnetic induction,

$\vec{E}$ = applied electric field,

e = charge on carrier,

$\left[\frac{\partial f}{\partial t}\right]_c$ = the rate of charge of f due to scattering of the carrier,

j = current density,

$\hbar = \frac{1}{2\pi} \times$ (Planck's constant),

and k = free carrier wave vector.

The coefficients defined by Equation 1.2 are elements of a generalized conductivity tensor and can be written as (3)

$$\sigma_{\eta\xi} = -\frac{e^2}{4\pi^3\hbar^2} \int d^3k \frac{\partial f}{\partial \mathcal{E}} \tau \frac{\partial \mathcal{E}}{\partial k_\eta} \frac{\partial \mathcal{E}}{\partial k_\xi}$$

$$\text{and} \quad \theta_{\eta\xi\sigma} = + \frac{e}{4\pi^3\hbar^4} \int d^3k \frac{\partial f_o}{\partial \mathcal{E}} \tau \frac{\partial \mathcal{E}}{\partial k_\eta} \frac{\partial \mathcal{E}}{\partial k_p} \frac{\partial}{\partial k_q} (\tau \frac{\partial \mathcal{E}}{\partial k_\xi})] \in_{\sigma pq} \qquad (1.3b)$$

where f_o = equilibrium distribution function of carriers,

$\mathcal{E}$ = electron energy,

τ = relaxation time of carrier,

and $\in_{\sigma pq}$ = permutation tensor.

In Equation 1.2 the elements linear in $\vec{B}$ give rise to the Hall effect (4) since the Hall voltage, induced at right angles to the constrained current flow in the presence of a magnetic field, is clearly related to $\theta_{\eta\xi\rho}$.

In case of spherical constant energy surfaces, $\mathcal{E} = \frac{\hbar^2 k^2}{2m}$, one obtains (5)

$$\sigma_{\eta\xi} = \frac{ne^2}{m} <\tau> \delta_{\eta\xi} \equiv \sigma_o \delta_{\eta\xi} , \qquad (1.4a)$$

$$\text{and} \quad \theta_{\eta\xi\rho} = - \frac{ne^3}{m^2} <\tau^2> \epsilon_{\rho\eta\xi} , \qquad (1.4b)$$

where n = free carrier concentration,

m = effective mass,

$$\text{and} <\tau^p> \equiv \frac{4}{3\sqrt{\pi}} \int_o^\infty dx x^{3/2} e^{-x} \tau p. \qquad (1.4c)$$

These results can be expressed as the conductivity tensor σ (B)

$$\sigma (B) = \begin{pmatrix} \sigma_o & \gamma B & -\gamma B_y \\ -\gamma B_z & \sigma_o & \gamma B_x \\ \gamma B_y & -\gamma B_x & \sigma_o \end{pmatrix} \qquad (1.5)$$

where σ_o is given by Equation 1.4a and

$$\gamma = - \frac{ne^3}{m^2} \langle \tau^2 \rangle .$$

If a time-dependent electric field which varies sinusoidally with angular frequency ω, $E(t) = E(o)e^{i\omega t}$, is introduced into the Boltzmann equation, the solution can be obtained simply by adopting the time-independent solution and substituting everywhere $\frac{\tau}{1 + i\omega\tau}$ for τ (6).

According to the Onsager relation (7), the linear terms in B in Equation 1.2 contribute antisymetrical elements to the conductivity tensor. These elements have an important effect at high frequencies due to this antisymmetrical property. In the physical situation, which corresponds to the actual experimental arrangement, the radiation propagates in a direction parallel to a cube axis (say the z axis) and B is in the direction of propagation, the conductivity tensor will in general be in the form of:

$$\sigma(B) = \begin{bmatrix} \sigma_{xx} & \sigma_{xy} & 0 \\ -\sigma_{xy} & \sigma_{yy} & 0 \\ 0 & 0 & \sigma_{zz} \end{bmatrix} \qquad (1.6)$$

The transformation

$$U = \begin{bmatrix} 1 & 1 & 0 \\ i & -i & 0 \\ 0 & 0 & 1 \end{bmatrix} \qquad (1.7)$$

diagonalizes σ with elements

$$\sigma_{11} = \sigma_{xx} + i\sigma_{xy}, \qquad (1.8a)$$

$$\sigma_{22} = \sigma_{xx} - i\sigma_{xy}, \qquad (1.8b)$$

and $\sigma_{33} = \sigma_{zz}$. (1.8c)

In the new expression $E_1 = E_x + iE_y$ and $E_2 = E_x - iE_y$ correspond to circularly polarized radiation, E_1 rotating clockwise, E_2 rotating counter-clockwise when viewed along the direction of the propagation. The propagation constants of E_1 and E_2 are determined by σ_{11} and σ_{22} respectively. They are

$$K^2 = \omega^2\mu\epsilon - i\omega\mu \begin{bmatrix} \sigma_{11} \\ \sigma_{22} \end{bmatrix} . \tag{1.9}$$

Since E_1 and E_2 are not equal, an incident plane polarized wave emerges from the crystal elliptically polarized with the major axis rotated through an angle with respect to the polarization of the incident wave. This rotation is the Faraday effect of free carriers. The effect is due to the influence of the magnetic field upon the translational motion of carriers and may thus be considered a distributed parameter extension of the Hall effect. It would then be expected that there is a close relationship between the Hall and Faraday effect through $\theta_{\eta\xi\rho}$. Stephen and Lidard (8) have pointed out that an explicit expression for the rotation angle can be given in terms of τ and the band structure constants by extending the usual calculation of the conductivity tensor ($B \neq 0$) to high frequency.

Since the frequency of infrared radiation is generally much higher than the collision frequency, the infrared Faraday effect gives information concerning the energy contours that is independent of the relaxation time (9). With microwaves, however, the radiation frequency and the collision frequency can be comparable. In this important frequency range,

the transport constants have both real and imaginary parts (see section IV., A.) and the complex Faraday effect yields added information concerning details of the scattering process. Because of the complex Hall terms, a microwave Faraday effect experiment also contains, potentially, more information than an ordinary d.c. Hall effect experiment.

B. Previous Work on Microwave Hall Effect Measurement

Various microwave experiments which permit the measurement analogous to that of Hall effect have been performed as mentioned in references (10) and (11). From observation at 20 GHz Hambleton and Gärtner (12) first reported the difference between the d.c. and microwave Hall mobility in germanium at low temperatures. Later, Watanabe (13) and Ho (11) also found a deviation between the microwave and d.c. Hall mobilities for both n-type and p-type germanium at low temperatures, but the discrepancy in the p-type samples was much larger than that in the n-type samples.

C. Band Structure of p-type Germanium (13)

The states of maximum energy in the valence band of germanium occur at $k = 0$ in the Brillouin zone and would be sixfold degenerate if there were no spin-orbit interaction. As a result of spin-orbit coupling, this level is split into a fourfold degenerate state at the top of the valence band and a doubly degenerate state, which is lowered by approximately 0.29 ev (14). Away from $k = 0$ the degeneracy of the upper band is lifted giving rise to two bands, the light hole and heavy hole bands. Holes are generally located at the center of the zone. Close to $k = 0$ both bands are parabolic, but away from $k = 0$ the assumption that $\mathcal{E} \propto k^2$

becomes a poor approximation for the light hole band (15). This departure from a parabolic behavior introduces a temperature dependence (as the distribution spreads in k space) into the transport properties; the ratio of light to heavy holes rises, the scattering probabilities of both carriers also rise (due to the increase in density of states) and the effective mass appropriate to the transport problem also becomes temperature dependent (16).

Directional cyclotron resonance measurements on germanium have revealed anisotropy in the energy surfaces of the valence states. The effect is small for the light hole band, but it is significant for the heavy hole band, where the effective mass ranges from 0.29 to 0.36 m_o (17, 18). Consequently, it is usual to refer to the energy surfaces of the heavy hole band as warped spheres. The general expression of the energy as a function of wave number for the valence bands of germanium near the band edge can be written as (19)

$$\mathcal{E} = \frac{\hbar^2}{2m_o}\left\{ Ak^2 \pm [B^2k^4 + c(k_x^2k_y^2 + k_y^2k_z^2 + k_z^2k_x^2)]^{1/2}\right\}, \qquad (1.10)$$

where x, y and z are referred to the cube axes, the positive sign to light holes, and the negative sign to heavy holes. A, B and c are dimensionless constants and can be related to the directional effective mass (20).

It should be recognized that the large difference in effective mass between the two kinds of holes may lead to relationships between the various transport properties which are significantly different from those of an equivalent set of carriers that have some suitably chosen single

mass (21).

D. Mobility of Holes

Existing information on scattering mechanisms in p-type germanium is very incomplete. The most extensive work in this field has been done in measuring the temperature dependence of the mobility. The strong temperature dependence of the mobility of p-type germanium, $u \propto T^{-2.3}$, was first observed by Lawrence (22) and confirmed by Prince (23). The mobility was obtained from direct resistivity measurements down to 100°K and was inferred from the observed temperature up to 500°K (24). This deviation in temperature dependence ($T^{-2.3}$) from $T^{-1.5}$ indicates that a simple acoustical mode scattering mechanism is inadequate to explain the actual physical phenomena. At the present time the origin of this high temperature dependence of mobility is not well established.

The factors which may complicate the problem are

(1) In any approach to quantitative considerations the warped nature of the heavy-hole band must be taken into account (25, 26).

(2) The contributions from impurity scattering must be taken into account, even for quite pure samples if the temperature is below 200°K. The results of Bray and Brown (27, 28) indicated that the mobility in high-purity p-type germanium at temperatures below 77°K can be accounted for by a mixture of acoustical mode and impurity scattering. Also, as pointed out by Becker (29) and Willardson and Beer (30), the impurity scattering should have a very strong effect,

particularly on the light hole band, in reducing its mobility even at low ionized impurity concentrations. Therefore, it may be necessary not only to treat the energy dependence of the relaxation time by a mixture of acoustical mode and ionized impurity scattering, but it may also be necessary to treat the impurity scattering on the light and heavy hole bands in different weight.

(3) There might be a possible change in effective mass with temperature. It should be noted that cyclotron resonance measurements have not been made above 100°K even in pure germanium (31, 32). However, some evidence showed that the light hole might increase their effective mass by at least 10 per cent in the temperature range from 2°K to 100°K. By contrast, the effective mass of heavy holes remained unchanged. One may therefore speculate on the possibility of a significant temperature dependence of the anisotropy parameters. The experimental methods for determining the effective mass at high temperature, which have proved to be successful for the electrons, are the infrared Faraday rotation (33) and reflection (34). However, because of the complication due to interband transition, these methods do not give the desired information for holes. Recently, Champlin et al. (35, 36) observed the conductivity effective mass, m_c^*, of holes in p-type germanium at 24 GHz throughout the temperature range between 90°K and 250°K and found that m_c^* was

significantly larger than the value 0.23 m_o calculated from cyclotron resonance data and increased rather markedly with temperature ($m_c^* \propto T^{0.7}$). If this result is true then, following Bagguley and Strandling's (31) cyclotron resonance experiment, one would expect the effective mass of the light holes to be very strongly temperature dependent.

(4) It is necessary to include optical phonon scattering of holes for, as both Harrison (37) and Bir and Pikus (38) have shown, there are non-vanishing zero order matrix elements for this interaction in germanium. Although this scattering can be expected to be of diminished importance at temperatures below liquid nitrogen (27, 28), yet at temperatures greater than 100°K it must be considered. In fact, it has been proposed as an explanation for the $T^{-2.3}$ phenomenon (39, 40, 41).

(5) When the impurity concentration is 10^{15} cm^{-3} or greater there are indications that hole-hole scattering is significant (42).

Theoretical considerations (13) have shown that any frequency dependence of the Hall mobility is closely related to the energy dependence of the relaxation time. In principle, measurement of the high frequency Hall effect can determine the relaxation time directly and thus contribute to our understanding of the $T^{-2.3}$ dependence of the mobility in p-type germanium. In practice, however, experimental and theoretical difficulties have not allowed relaxation times to be obtained in this way.

E. Purpose of Investigation

As mentioned previously several investigators found that the deviation between the d.c. and microwave Hall mobilities for p-type germanium did really exist and that the difference was very large at low temperatures. According to Watanabe's (13) conclusion, any high frequency effect existing in the Hall mobility must be caused by the combined effect of the energy dependence of the relaxation time and of $\omega\tau \geq 1$. Therefore, this difference between d.c. and microwave mobilities must be closely related to scattering mechanisms in the sample although there may also be some other high frequency effects.

In the present investigation an effort has been made

(1) to develop a system such that the measurement of the temperature dependence of the microwave Hall mobility can be extended from liquid nitrogen temperature (11) to liquid helium temperature,

(2) to study the effect of impurity scattering on the difference between d.c. and microwave Hall mobilities in p-type germanium at temperatures ranging from liquid helium to room temperature.

II. EXPERIMENTAL PROCEDURE

A. Microwave Measurement

1. Principle of microwave measurement

The microwave degenerate cavity system (Fig. 1) and the power relationship for the arrangement have been studied in detail by Nishina and Danielson (43) and by Liu *et al.* (44). As shown in Fig. 1, a square semiconductor sample of the linear dimension ℓ is placed at the center of the end wall of the cavity and is parallel to the xy plane. The cavity can have only the lowest two distinct modes of resonant oscillations at a single microwave frequency, namely the TE_{101} mode and the TE_{011} mode.

If the microwave power P_1 at resonant frequency is incident on the cavity through one branch of the waveguides (say branch I) and excites the TE_{101} mode of oscillation in the cavity, then when a static magnetic field B is applied in the z direction, the Hall effect in the sample will excite the TE_{011} mode of oscillation in the cavity with power P_2. A part of the power P_2 will be coupled out to the other waveguide. Thus $\frac{P_2}{P_1}$ is a function of the static magnetic field, sample geometry, conductivity, dielectric constant, and the Hall mobility.

Theoretical analysis gives the relationship (44)

$$\sqrt{\frac{P_2}{P_1}}\ \frac{1}{|1+R|} = \left|\frac{\eta + \alpha B_o u + i(\eta' + \alpha B_o u)}{Y_o + G + 2\alpha + 2i(x+\alpha)}\right| \qquad (2.1)$$

where P_1 = microwave power incident on the cavity to excite the TE_{101} mode,

P_2 = microwave power out of the TE_{011} mode in the cavity,

R = reflection coefficient for the power P_1 at the iris plane,

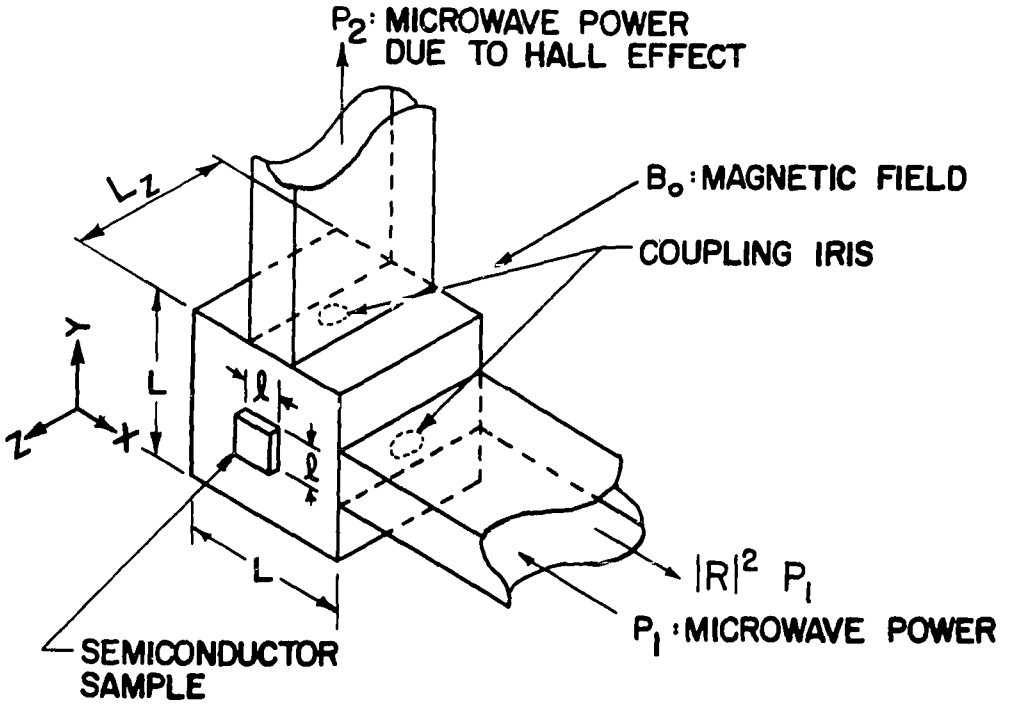

Fig. 1. Principle of microwave Hall mobility measurement

$\alpha = \frac{1}{L_z} \left(\frac{2}{\omega\mu\sigma_o}\right)^{1/2} \frac{\bar{\ell}^2}{L^2 + L_z^2}$, $2\alpha = \frac{1}{Q_s}$ where Q_s is the Q of the cavity due only to the loss in the sample,

σ_o = d.c. conductivity of the sample = eNu_o,

$u = \frac{e\tau}{m} \frac{1}{1 + i\omega\tau}$ = mobility with the effect of relaxation time,

N = density of carriers,

L_z = dimension of the cavity in the z direction,

$\bar{\ell}$ = effective linear dimension of square sample,

L = dimension of the cavity in the X or Y direction,

μ = permeability of the sample,

$\eta + i\eta'$ = mutual admittance to represent the coupling due to the non-ideality of the cavity,

$x = \frac{\omega - \omega_o}{\omega_o}$,

ω = microwave angular frequency,

ω_o = resonant frequency of the TE_{101} and the TE_{011} mode,

Y_o = characteristic admittance of the waveguide in the units of ωc, where c is the capacity of the resonant circuit corresponding to the TE_{101} or TE_{011} mode (Y_o is the reciprocal of the external Q),

and G = conductance representing the loss in the cavity wall in units of wc (G is the reciprocal of the unloaded Q without sample).

All quantities are expressed in MKS units.

Equation 2.1 was derived with the assumptions:

(1) There is only one kind of carrier with isotropic effective mass m, and relaxation time τ.

(2) The static magnetic field is weak so that $|B_o u| << 1$.

(3) The sample size is relatively small compared to the

dimensions of the cavity.

(4) The field distribution inside the sample is approximated by a plane wave. The microwave electric field is then uniform over the sample surface except at the boundary to the cavity wall where it suddenly drops down to almost zero.

If Equation 2.1 is expressed in terms of the conductivity tensor of a sample, the result can then be extended to the case of two types of carriers and to an arbitrary shape of the energy surfaces (10). If some simplified assumptions are made, Equation 2.1 can be applied to p-type germanium, which has two types of carriers (light holes and heavy holes).

Experimentally, the nonideal coupling between the TE_{101} mode and the TE_{011} mode was effectively cancelled, so that $\eta + i\eta' = 0$. Also, the frequency deviation $x = \frac{\omega-\omega_c}{\omega_o}$ was chosen to maximize the relative power output P_2, so that the imaginary part of the denominator on the right hand side of Equation 2.1 was approximately zero.

Equation 2.1 is then reduced to (44)

$$\left(\frac{P_2}{P_1}\right)^{1/2} \quad \frac{1}{|1 + R|} \quad \frac{\sqrt{2}\alpha \; B_o \; u_o}{Y_o + G + 2\alpha} \cdot \frac{1}{(1 + i\omega\tau)} \tag{2.2}$$

where $u_o = \frac{e\tau}{m}$ = mobility of the charge carriers given by a d.c. method,

and α = one-half the reciprocal of the Q of the cavity due only to the loss in the sample.

2. Microwave cavity system

The actual structure of the rectangular degenerate cavity system is shown in Fig. 2. The main body of the cavity was made of brass. The

Fig. 2. Cavity construction for low temperature measurement

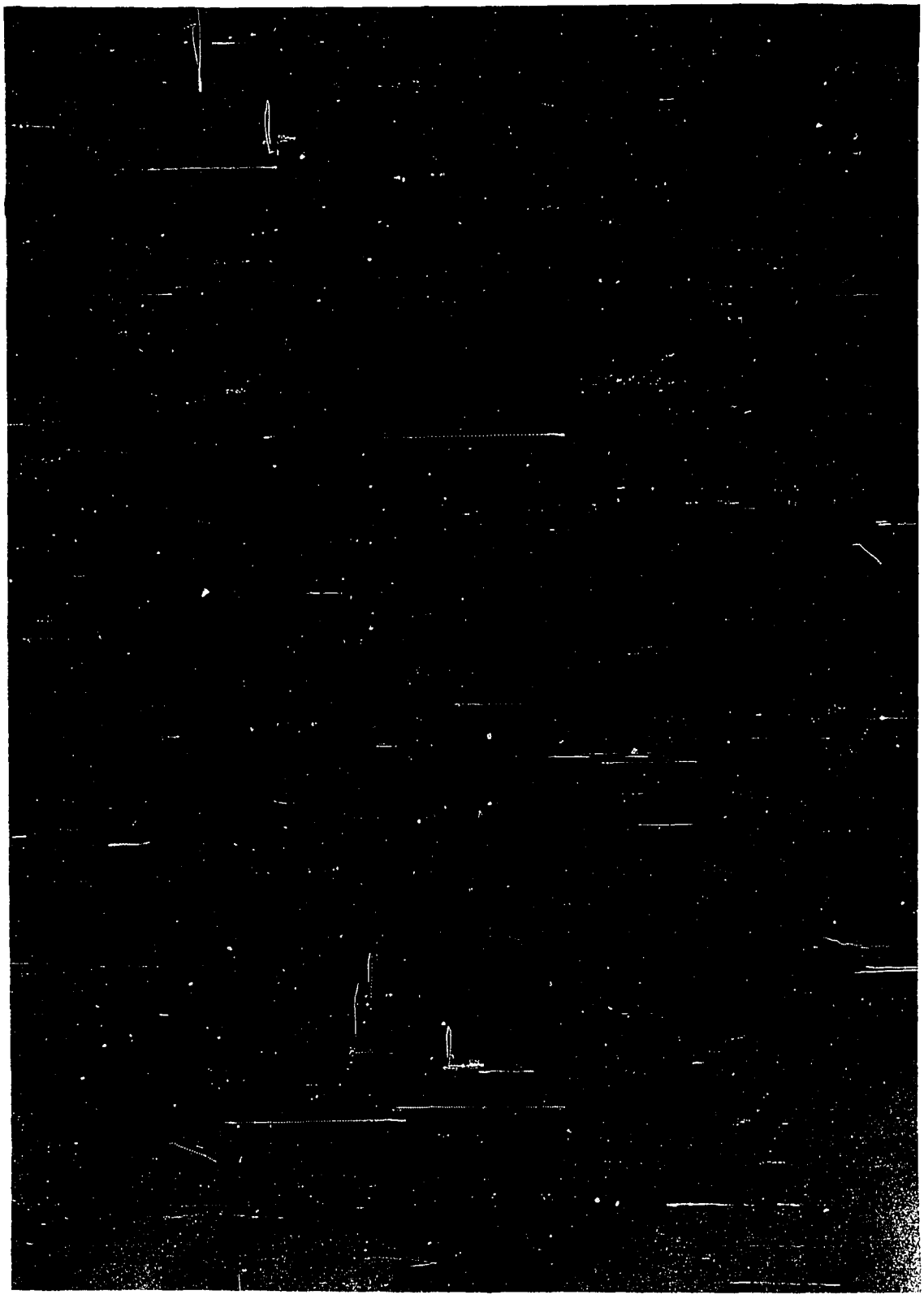

inside of the cavity was plated with gold. Two short sections of brass waveguide with sharp 135° angle were used to couple the cavity through the coupling iris to two thin-walled stainless steel waveguides at the other ends. The interior of the stainless steel waveguides were plated with silver. Maintenance of the temperature difference between the room and the cavity was accomplished through the use of two stainless steel waveguides each about three feet long. A brass flange to a vacuum chamber was used as the mechanical support for the two waveguides and the cavity.

The degeneracy of the cavity was adjusted by two tuning screws placed at the centers of the cavity walls. Also the non-ideal coupling between the TE_{101} mode and the TE_{011} mode was reduced by another two screws which were set at the corners of the cavity. The cavity and the stainless steel waveguide were completely enclosed in the vacuum chamber of the cryostat so the heat leak due to convection might be reduced to minimum.

A plastic plate of thickness 1/16" was inserted with an O-ring between the flanges to the stainless steel waveguide and the flange to the waveguide outside the vacuum chamber so that the stainless steel waveguides could be vacuum-sealed. The reflection due to the plastic window was compensated with three screw stubs which were placed on a piece of waveguide in approximately a quarter wavelength separation.

The power reflected by this plastic window under the matching condition and the shift in resonant frequency of the cavity due to the stubs were very small and can be neglected within the accuracy of the measurement (10).

3. Cryostat system and temperature control

The cryostat shown in Fig. 3 was of common design, having two chambers for liquid refrigerant which were isolated from each other and from the outside by vacuum chambers.

The cavity was located at about the middle position of the tail of the sample chamber which could either be vacuum-tight or be filled with exchange gas to increase the thermal contact between the cavity and the coolant.

The temperatures of the sample below 25°K were measured with an Au 0.07 at % Fe vs. Cu thermocouple calibrated by Finnemore et al. (45) and above 25°K with a Cu vs. constantan thermocouple (46). These thermocouple wires were soldered on the cavity block. The thermocouple voltage was measured with a Leeds and Northrup 8687 potentiometer.

In case of the liquid helium measurement the following precooling procedure was taken:

(i) The liquid nitrogen chamber was first filled with liquid nitrogen.

(ii) The sample chamber and the vacuum jacket between the liquid helium and liquid nitrogen chambers were then isolated from the vacuum system.

(iii) A small amount of hydrogen gas was introduced into the sample chamber (as well as the liquid helium chamber) as exchange gas.

(iv) The temperatures of the system reached equilibrium after two hours, the hydrogen gas was then pumped out from the vacuum jacket.

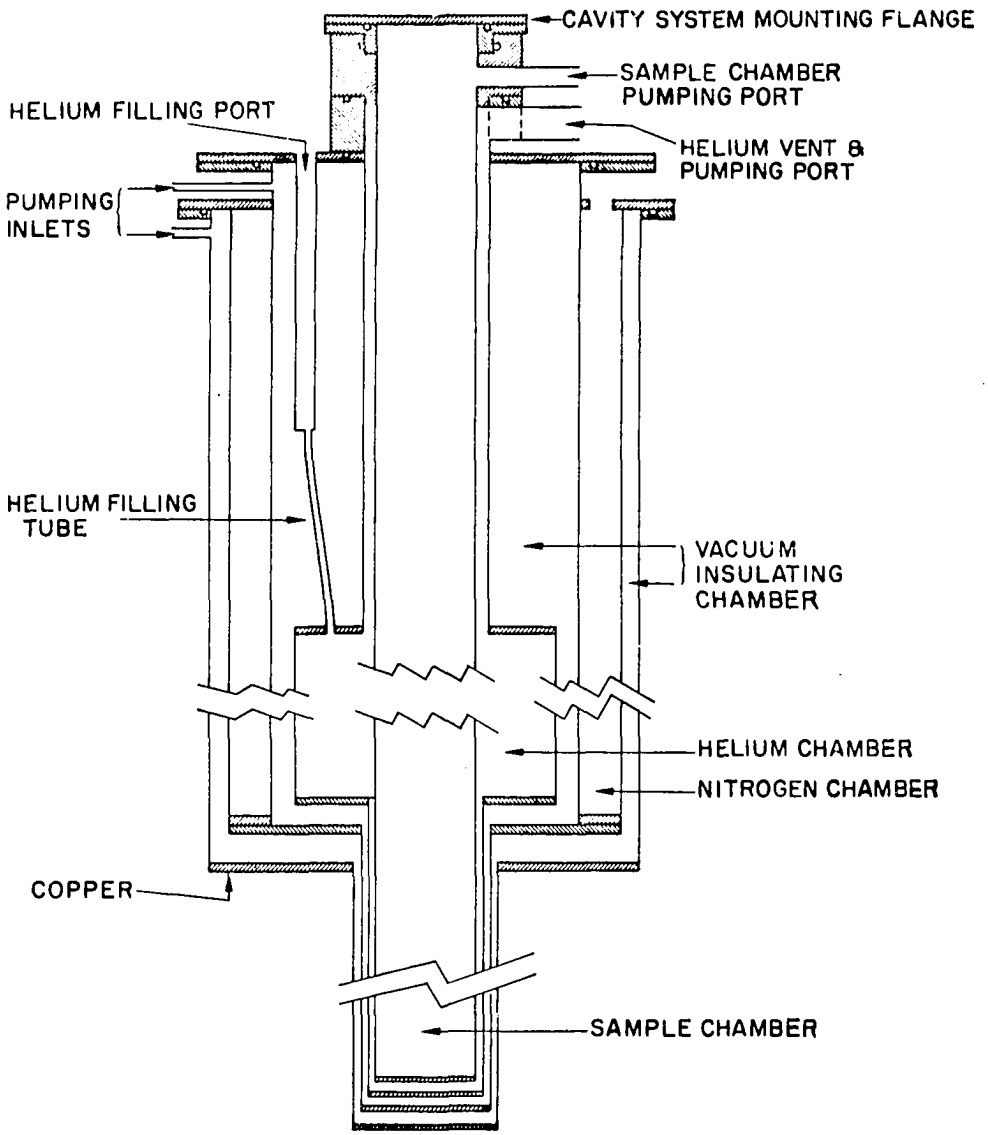

Fig. 3. Cryostat

(v) The liquid helium was transferred into the liquid helium chamber.

The reason for using hydrogen gas as the transfer gas in the vacuum jacket was that a high vacuum between the liquid helium and liquid nitrogen chamber was required in order to reduce the loss of liquid helium. Since the hydrogen molecule is lighter than the nitrogen and helium molecules, it was easier to pump out hydrogen and heat loss was reduced to a minimum. This precooling procedure was different from the ordinary one in that the liquid helium chamber was not initially filled with liquid nitrogen because the helium transfer tube of the present cryostat was not made to reach the bottom of the chamber. Thus, if the liquid nitrogen was used for precooling it could not be completely forced out by helium gas and would take a very long time for its complete evaporation before the liquid helium could be transferred.

Eight liters of liquid helium were required to fill the cryostat after precooling. If the exchange gas was controlled properly the cavity temperature can be brought down to about 5°K and the liquid helium will last for about six hours.

The temperature control is made by adjusting the gas pressure of the exchange gas in the sample chamber and the current through the heater wire which was wound on a copper tube attached to the cavity at the bottom (see Fig. 2).

4. Sample preparation

The single crystals of p-type germanium of different impurity concentrations were obtained from Texas Instruments Company. The samples

were cut to the size of about 10 mm x 10 mm x 3 mm. The square edges of the sample surface were oriented in the <100> and <010> directions so that the crystal could be placed in a position symmetrical to both of the TE_{101} mode and TE_{011} mode of the microwave fields.

The sample was mounted on one side of the cavity walls with silver paint as shown in Fig. 2 and was further pressed against the frame with another brass plate. The silver paint kept the sample in good thermal and electric contact with the cavity wall.

5. Microwave measurement procedures

The microwave system is shown in Fig. 4. A Strand Laboratories, Inc.[1] X-band microwave generator with an average power output of about 20 milliwatts was used. This oscillator consisted of a klystron, a ferrite isolator, a stabilization discriminator, and a reference cavity. The ferrite isolator isolated the klystron from the outside circuit so that the klystron could operate without being affected by changes in the impedance of the microwave load. The frequency was stabilized to the tunable reference cavity.

The measuring system was the same as that described by Nishina (10) except for the method of modulation. The microwave signal was modulated by a 1000 cycles per second square-wave signal. The modulation was performed by a section of a semiconductor switch/modulator/attenuator[2].

---

[1]Strand Laboratories, Inc., 294 Center Street, Newton 58, Mass.

[2]Somerest Radiation Laboratories, Inc., 192 Central Ave., Stirling, New Jersey.

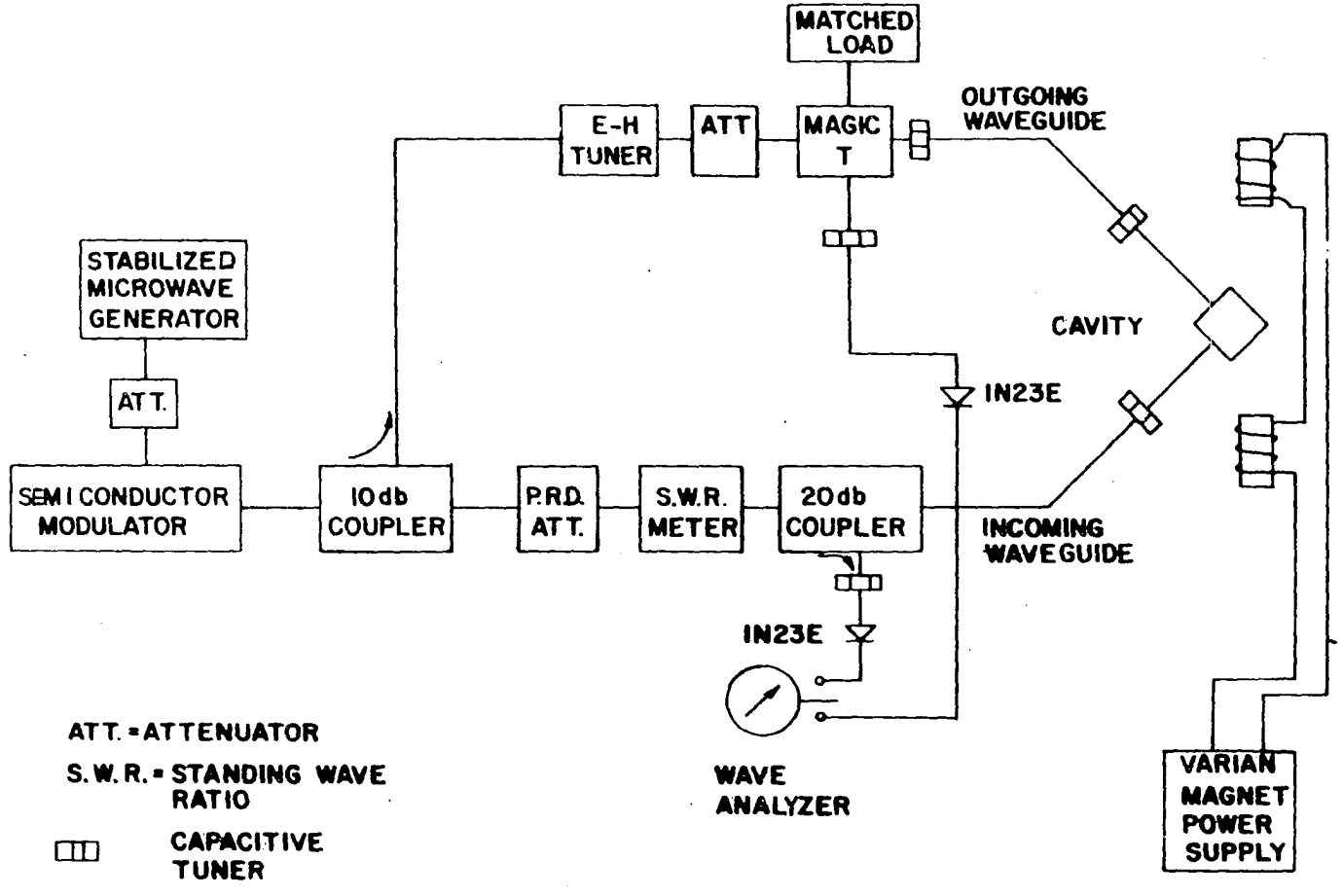

Fig. 4. Schematic diagram of microwave circuit

The modulator was made in the form of a section of waveguide inserted in the microwave circuit before the 10 db coupler. The modulating action depended upon the increase in energy absorption resulting from the increase in conductivity caused by the injection of excess minority carriers. By modulating the conductivity of the semiconductor crystal one could obtain a change in the microwave energy transmitted through the system. This method of modulation had two advantages:

(1) The signal was nearly free from phase or frequency modulation.

(2) The modulation did not affect the r.f. oscillator, so fluctuation of the r.f. was kept to a minimum.

The microwave power detected by the diode was then amplified and measured by a wave analyzer.

The procedure for the microwave measurements was as follows. First, the sample-loaded cavity was adjusted to the degenerate state. The non-ideal coupling between the TE_{101} and TE_{011} mode was reduced to a minimum by adjusting the screws at the corners of the cavity. The residual part of the non-ideal power output of the cavity was then cancelled out at the magic T detector by adjusting the E - H tuner and the attenuater in the bridge circuit between 10 db directional coupler and the magic T. This adjustment allowed the coherent wave out of the 10 db directional coupler to have the proper magnitude and phase as it reached the magic T. After the cancellation of the non-ideal power, a static magnetic field was applied.

The reading of the P.R.D. attenuator was set to zero at the beginning of the measurement. As the static magnetic field was applied, the output

detector detected a signal which was related to the microwave Hall power P_2 shown in Equation 2.1. This signal was read on the wave analyzer in an arbitrary scale. The signal corresponding to the input power was then measured from the detector at the 20 db directional coupler by tuning P.R.D. attenuator to such a value (say α_1 db) that the wave analyzer gave the same reading as that for the output signal. In order to get the actual output to input power ratio, the output of the magic T detector must be calibrated with respect to the output of the detector at the 20 db coupler. This calibration was performed by removing the cavity and by directly connecting a piece of waveguide in half-circled shape between the E-arm of the magic T and the main guide of the 20 db coupler. The attenuation of the P.R.D. (say $\alpha_2$db) with the same reading at the two detectors was recorded. The power ratio was then given by the relation

$$10 \log \frac{P_1}{P_2} = \alpha_1 + \alpha_2 \qquad (2.3)$$

B. d.c. Measurement

The d.c. conductivity and Hall coefficient measurements were performed with a cryostat and sample holder similar to those used by Zrudsky (47).

The samples for the d.c. measurement were cut with a diamond saw from the same crystals immediately adjacent to those parts which were cut for microwave measurement. The crystals were cut along their rectangular edges in the <100>, <010>, and <001> directions. The dimensions of the samples were measured by Gaertner traveling microscope[1].

---

[1]The Gaertner Scientific Corp., Chicago, Illinois.

Three probes were used for these measurements. The details of the probe arrangement and voltage relations have been discussed by Heller (48). It was found after testing that the values of conductivity and mobility were erratic due to the high contact resistance between the probes and the sample. In order to reduce this contact resistance, the sample surface, with which the probes were in contact, was covered with Zn-10[1] by means of an ultrasonic solder gun. The following procedure was used to minimize the uncertainty in measuring the distance of the probe separation owing to the presence of the soldered spot.

(1) The resistance of the sample for an arbitrary distance of separation was first measured with a Leeds and Northrup Model 7553, Type K-3 potentiometer on a special sample holder designed for room temperature measurement. The distance of separation was measured with a traveling microscope before the spots of contact were covered with Zn-10.

(2) The sample with the soldered Zn-10 spots was mounted on the low temperature sample holder and the resistivity and Hall coefficient were measured. The resistance obtained at room temperature was used to calculate the distance of separation of the resistance probes by comparing with the resistance obtained in procedure 1 at the same temperature.

The Hall voltage and the resistivity drop were measured by an integrating digital voltmeter.

---

[1] 10% Zn, 90% Sn.

III. EXPERIMENTAL RESULTS

A. Field Dependence Measurement

In order that the Hall measurement can be operated in such a field region that the low field approximation of Equation 2.2 can be applied properly and the system can still give a detectable signal, the field dependence of the Hall power ratio ($\sqrt{\frac{P_2}{P_1}}$) of the p-type germanium samples was first measured at room (300°K), liquid nitrogen (78°K), and near liquid helium (5.5°K etc.) temperatures, respectively. From these data, then, a suitable magnetic field strength was chosen in the study of the temperature dependence of the Hall mobility for the same samples.

Figure 5 shows the magnetic field dependence of $\sqrt{\frac{P_2}{P_1}}$ of three p-type germanium single crystals (439HGP, GP1, and 439GP) at the three different temperatures as mentioned above. The curves show that the Hall power ratio deviates from linear relationship with respect to the magnetic induction B at higher fields and that this deviation becomes more pronounced and starts at lower field intensity with decrease in temperatures especially at near liquid helium temperatures. As shown in the curves, the power ratio started to deviate from linear relationship at about 0.35 wb/m^2, 0.3 wb/m^2, and 0.23 wb/m^2 at room temperature, liquid nitrogen, and near liquid helium temperatures respectively. This phenomenon is probably due to the light holes in a p-type crystal as explained by Willardson *et al.* (21). From these values the static magnetic field was chosen at 0.2 wb/m^2 for the Hall measurements for all samples under investigation. This magnetic field intensity was considered weak throughout the whole range of temperatures studied.

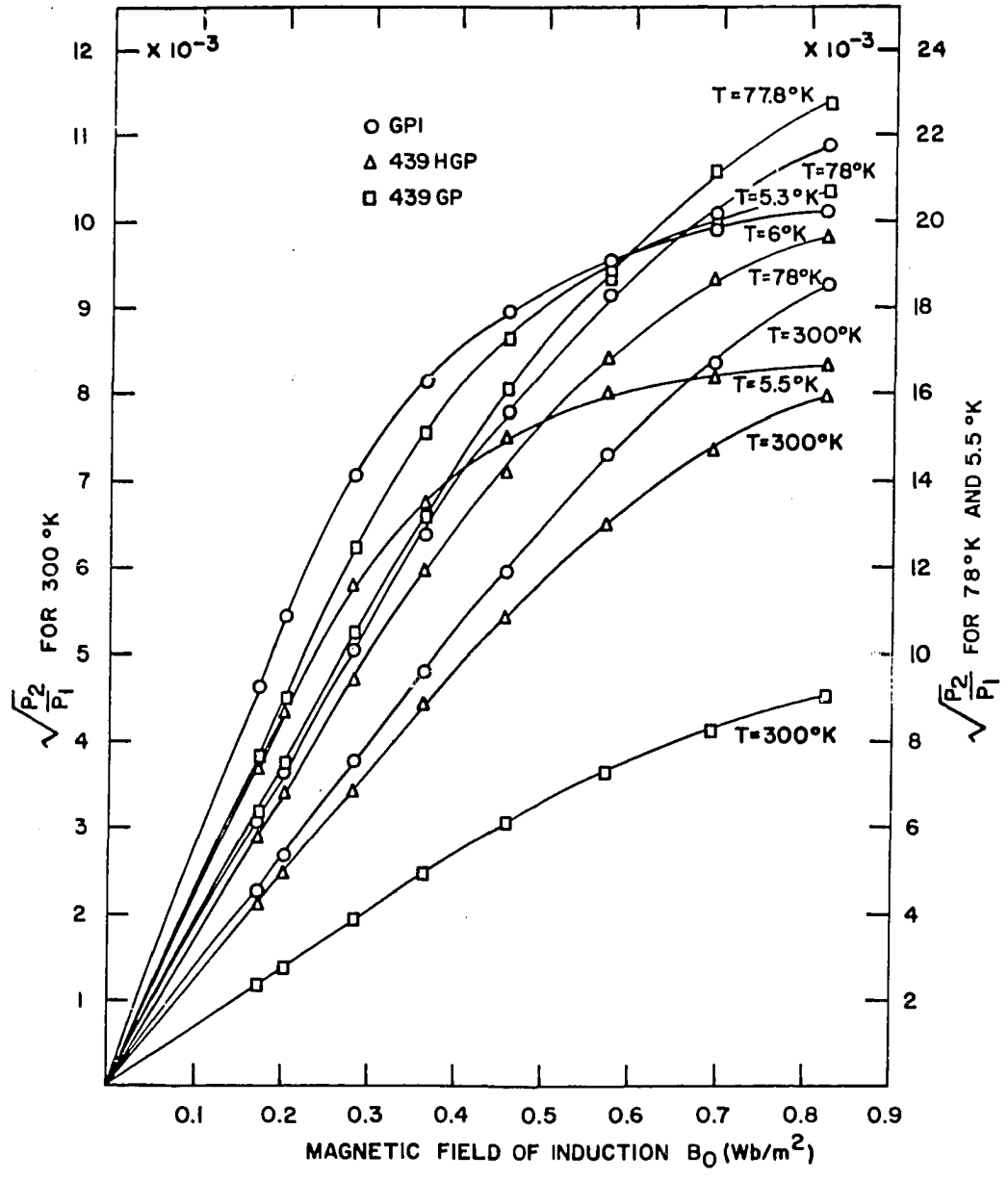

Fig. 5. Magnetic field dependence of $\frac{P_2}{P_1}$ for p-type germanium single crystals

B. Temperature Dependence Measurement

The temperature dependence of the microwave Hall mobility was calculated from Equation 2.2. First an α value (2α = the reciprocal of the cavity Q given by the losses in the sample) was chosen in such a way as to give the best agreement between the d.c. and microwave mobility values at room temperature. This value of α was used to determine the effective sample size $\bar{\ell}$. The reason for choosing the effective sample size in this manner can be explained as follows. According to the definition of α($\alpha = \frac{1}{L_z}\left(\frac{2}{\omega\mu\sigma}\right)^{1/2} \times \frac{\bar{\ell}}{L + L_z}$) the term $\bar{\ell}$ is an effective dimension of the sample on the cavity wall which not only depended upon the actual sample size but also on the physical contact between the sample and the cavity wall. Since the condition of physical contact was not reproducible it was impossible to give a definite proportional constant between the effective sample size $\bar{\ell}$ and the actual sample size ℓ. However, the relaxation time decreased appreciably with increase in temperature due to the increase in lattice scattering. Hence, any high frequency effect which existed at low temperatures would gradually diminish at higher temperatures. The relaxation time of p-type germanium was approximately equal to 10^{-11} sec (20) at liquid helium temperature and $\omega\tau \sim 1$ under the frequency of 10 GHz. Thus, one would expect that $\omega\tau << 1$ and the high frequency effect would become insignificant at room temperature. The correction factors calculated were 0.496, 0.845, 0.792 and the effective sample size $\bar{\ell}$ then became 9.0 X 0.496 = 4.47 mm, 9.7 X 0.845 = 8.20 mm, and 9.1 X 0.792 = 7.21 mm for samples 439HGP, GP1, and 439GP respectively. These $\bar{\ell}$ values were used in the calculation of α at

different temperatures. The temperature dependence of α was assumed to be inversely proportional to the square root of the d.c. conductivity of the same sample.

The characteristic admittance Y_o of the waveguide was found from the loaded Q of a nondegenerate cavity without the sample and from the reflection coefficient of the cavity at resonant frequency in the plane of the cavity iris. The Y_o value so calculated was equal to 9.87×10^{-4} and was assumed to be constant over the whole temperature range, since the characteristic impedance of the waveguide was practically independent of the temperature of the cavity and the electromagnetic energy stored in the cavity was determined once the cavity dimensions and the field amplitude were given.

The reciprocal of the loaded Q of the cavity with the sample, $Y_o + G + 2\alpha$, was given from the relationship

$$Y_o + G + 2\alpha = Y_o \frac{2}{|1 + R|} ,$$

where the reflection coefficient R of the cavity was measured at the resonance frequency. The argument of R was determined from the difference in the position of the standing wave minima when the input iris to cavity was opened and closed with a brass plate. It was impossible to determine $Y_o + G$ from the Q of the cavity without a semiconductor sample because of the following reasons.

(1) When a part of the cavity wall was replaced by a different material with resistivity higher than that of the cavity wall by a factor of 10^5 or greater, the microwave field distribution on the wall was perturbed appreciably so

that G would not be the same as that without the sample.

(2) The Q value of the cavity was very sensitive to how the sample frame was placed in contact with the main body of the cavity. Once the frame was removed, it was difficult to obtain a reproducible Q value.

Since the skin depth δ is inversely proportional to the square root of the conductivity [$\delta = (\pi f \mu \sigma)^{-1/2}$], the largest value of the skin depth of the samples would occur at room temperature (in the extrinsic region the conductivity of semiconductor increases as the temperature decreases). The skin depth of samples 439HGP, GP1, and 439GP were 1.16 mm, 1.33 mm, and 0.32 mm respectively at room temperature and the corresponding thickness of the samples were 3.3 mm, 3.5 mm, and 2.4 mm respectively. Hence, the ratio of sample thickness to skin depth of the samples was at least greater than 2.5 and it was reasonable to assume that the field was completely attenuated inside the sample as the microwave field propagated through the sample.

Figure 6 showed that the microwave Hall mobility of sample 439GP started to deviate from its d.c. Hall mobility at about the same temperature (about 200°K) as in sample GP1, and this deviation appeared at a much higher temperature than that in sample 439HGP (about 150°K). The difference between the d.c. and the microwave mobilities at low temperatures became greater in the order of 439GP > GP1 > 439HGP as shown in Fig. 7 in terms of per cent deviation, whereas the purity of the samples followed the opposite order 439HGP > GP1 > 439GP as shown in the resistivity curves (Fig. 8). This result clearly indicates that impurity in

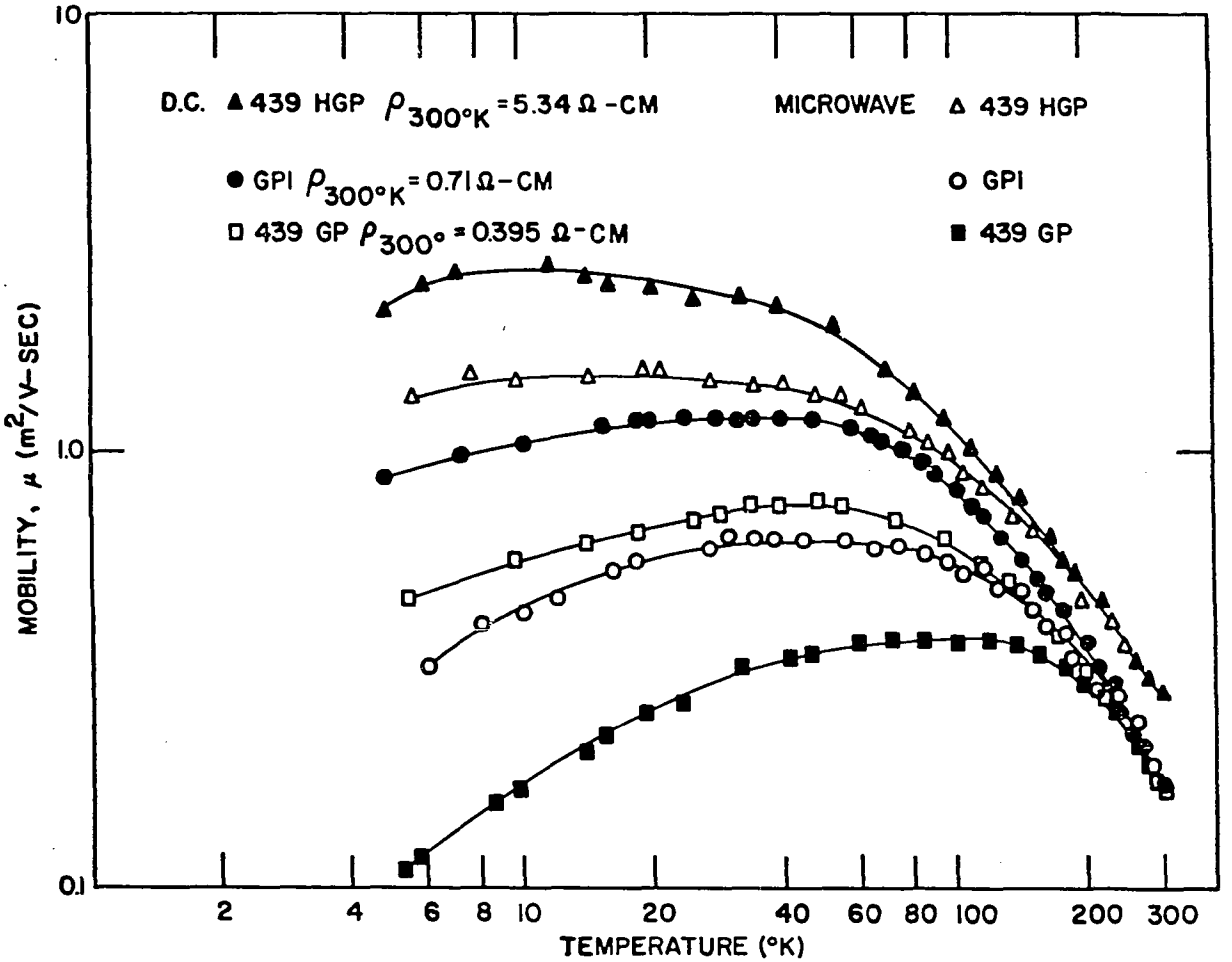

Fig. 6. Hall mobility of p-type germanium single crystals vs. temperature

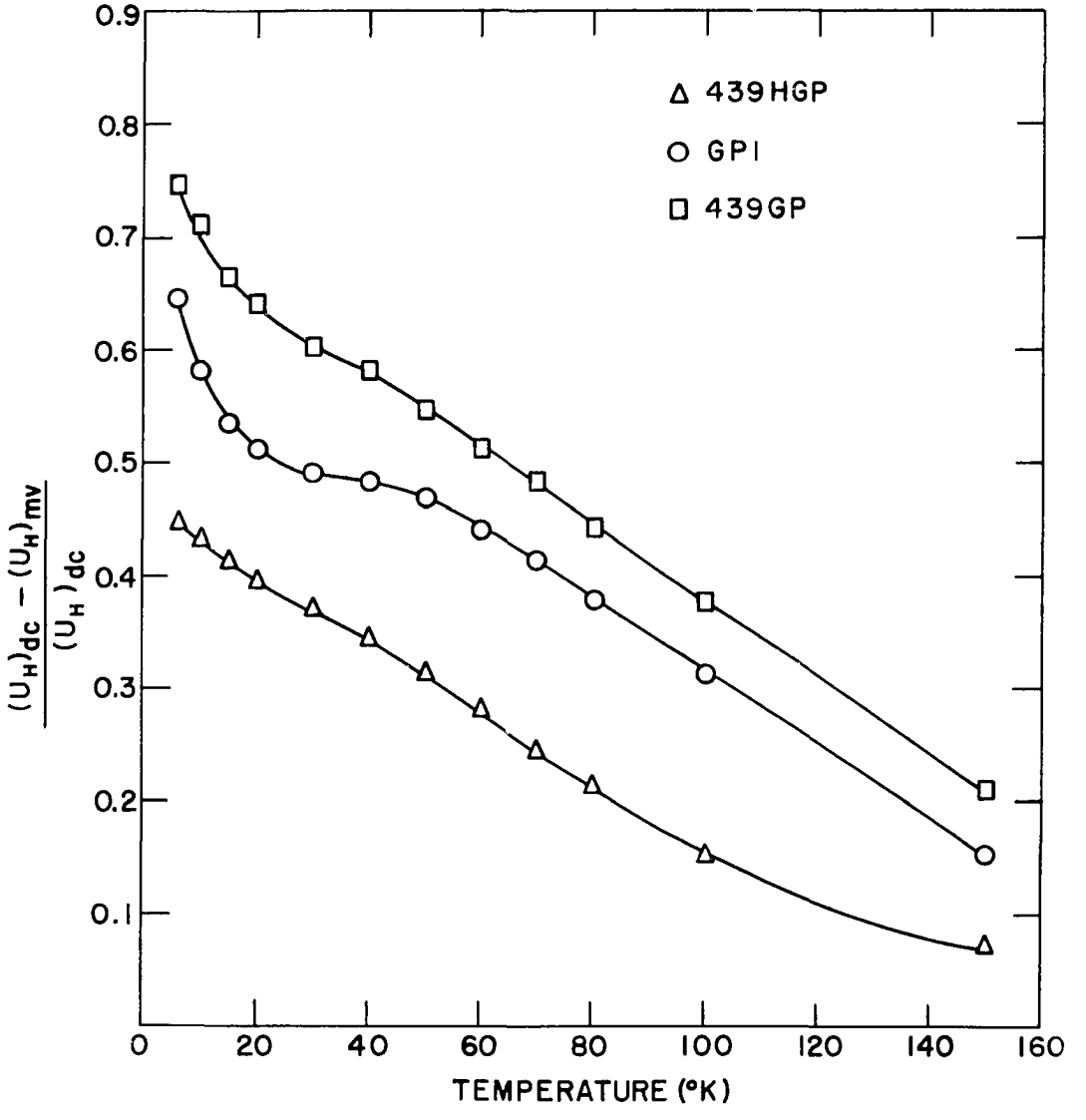

Fig. 7. $\frac{(u_H)_{dc} - (u_H)_{dc}}{(u_H)_{dc}}$ vs. temperature

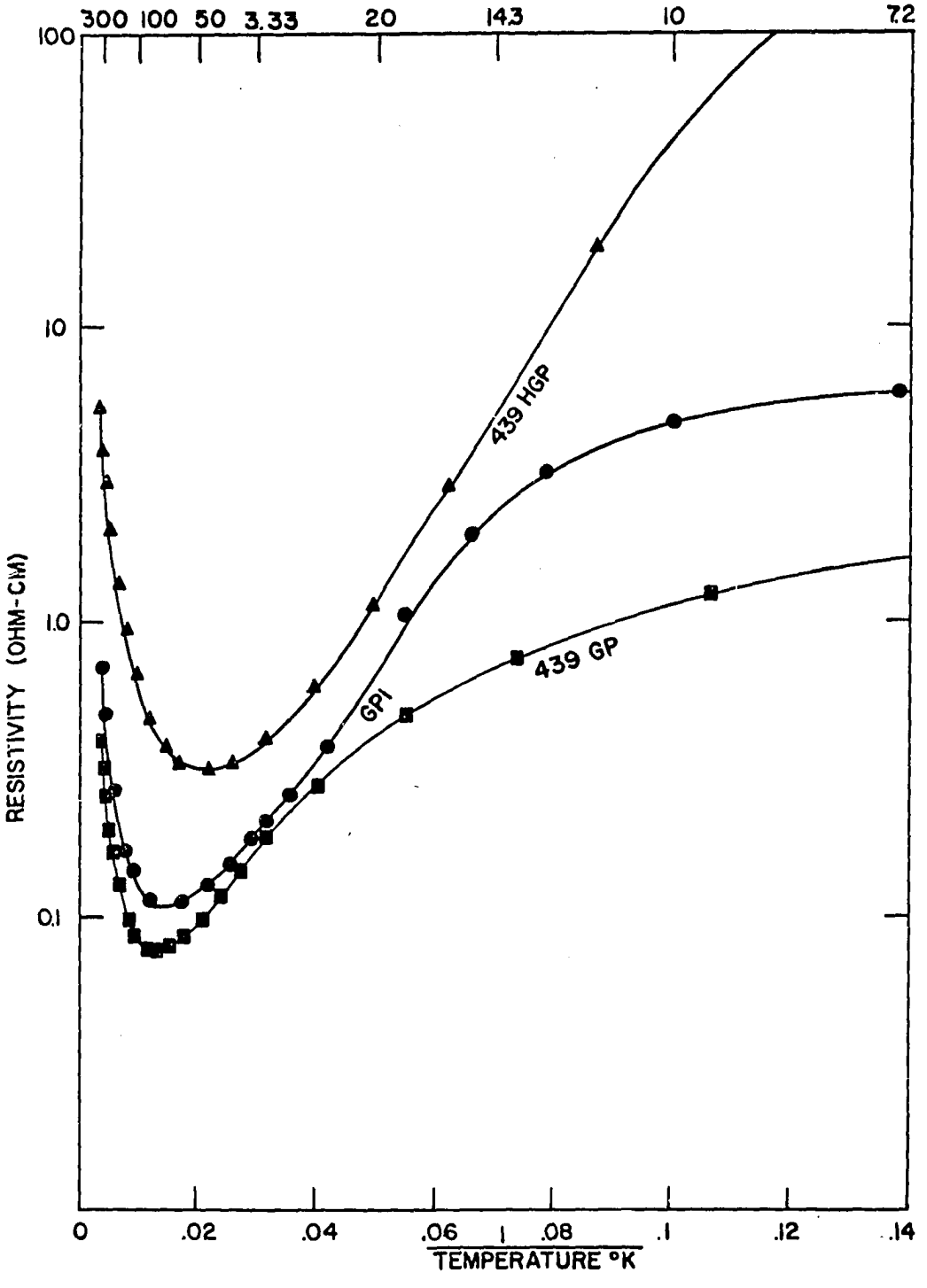

Fig. 8. Resistivity of p-type germanium single crystals vs. reciprocal of temperature

the sample definitely has some effect on the difference between the d.c. and microwave mobilities.

IV. DISCUSSION

A. Charge Carrier Inertia

The considerable difference between the microwave and the d.c. Hall mobilities at low temperatures may be attributed to

(1) the carriers inertial effect, and

(2) the combined phonon and impurity scattering.

The response of charge carriers to a rapidly varying electric field becomes limited at high frequencies due to the inertia of the carriers and results in an out-of-phase component of motion between the charge carriers and the applied field. If we introduce the concept of relaxation time and effective mass into the motion of free carriers in a solid, the semi-classical equation of motion for carriers may then be written in the form

$$m\left(\frac{d\vec{v}}{dt} + \frac{1}{\tau}\vec{v}\right) = \vec{F} \qquad (4.1)$$

as first proposed by Dresselhaus et al. (20), where $\vec{F}$ is the average external force acting on a carrier. The term $\frac{m}{\tau}\vec{v}$ has the form of a frictional or damping force, with $\frac{m}{\tau}$ playing the part of a coefficient of friction, and the term $m\frac{d\vec{v}}{dt}$ describes inertia effects and should be included in problems where the applied field is time-dependent. In case the field is varied as $e^{i\omega t}$, Equation 4.1 becomes

$$m\left(i\omega + \frac{1}{\tau}\right)\vec{v} = \vec{F} \qquad (4.2a)$$

or

$$m(1 + i\omega\tau)\vec{v} = \tau\vec{F} \qquad (4.2b)$$

It is then clear from Equation 4.2b that the term $\omega\tau$ is associated with

the carrier inertia and that the inertial effect is frequency and energy dependent (τ is energy dependent). Physically, at frequencies such that $\omega\tau >> 1$ the free carriers undergo many oscillations without any scattering interaction with their surroundings. In the absence of scattering interaction the carriers would move out-of-phase with the applied field, and no power would be dissipated. As the frequency is lowered the out-of-phase motion becomes increasingly hindered by scattering processes until, at sufficiently low frequencies ($\omega\tau << 1$), the out-of-phase motion becomes insignificant in comparison with the in-phase motion due to the damping produced by scattering. These in-phase and out-of-phase motions of charge carriers result in the conductivity as a complex function of frequency. The in-phase component contributes to the real conductivity and the out-of-phase component contributes to the permittivity. Thus, the most interesting effects are expected to be at frequencies such that $\omega\tau \gtrsim 1$.

To simplify the mathematical analysis and to provide a preliminary explanation of the experimental results, let us consider the transport coefficients σ and θ in Equation 1.2. If we assume that the band structure is a nondegenerate single-valley centered at k = 0, the high frequency dependence of these coefficients could be written as (49)

$$\frac{\sigma(\omega)}{\sigma(0)} = \frac{\langle\tau/(1 + i\omega\tau)\rangle}{\langle\tau\rangle} \tag{4.3}$$

$$\frac{\theta}{\theta(0)} = \frac{\langle\tau^2/(1 + \omega\tau)^2\rangle}{\langle\tau^2\rangle} \tag{4.4}$$

normalized with respect to the d.c. values. The real and imaginary parts

of Equation 4.3 and 4.4 evaluated as function of $\omega\langle\tau\rangle$ for the case of Maxwell-Boltzmann distribution and $\langle\tau\rangle$ = constant (neutral impurity scattering) (50), $\tau \propto^{-1/2}$(acoustic mode scattering) (51), and $\tau \propto {}^{3/2}$ (ionized impurity scattering) (52) are shown in Fig. 9 and 10. From these figures one notices that

(1) any deviation from a constant relaxation time will move frequency-dependent effect to correspondingly lower frequencies,

(2) the high frequency effect will always reduce the real part of conductivity to a value smaller than d.c. conductivity, and

(3) for the same $\omega\langle\tau\rangle$, the real part $\frac{\sigma(\omega)}{\sigma(0)}$ corresponding to impurity scattering is less than the value corresponding to lattice scattering.

Since the real part of conductivity associates with the energy dissipated by carriers, and the microwave Hall mobility is proportional to $\sqrt{\frac{P_2}{P_1}}$, as given in Equation 2.1 (P_2 related to the energy absorpted by the carriers), one would deduce from the above arguments that the microwave mobility will always be lower than the corresponding d.c. value when $\omega\tau \gtrsim 1$ and that the difference between the microwave and d.c. mobilities will become greater with increasing impurity scattering. If we consider the combined lattice and impurity scattering one would expect the curve of Re $\frac{\sigma(\omega)}{\sigma(0)}$ to be at somewhere between the curves due to pure lattice scattering and pure impurity scattering. This conclusion agrees qualitatively with the present experimental result.

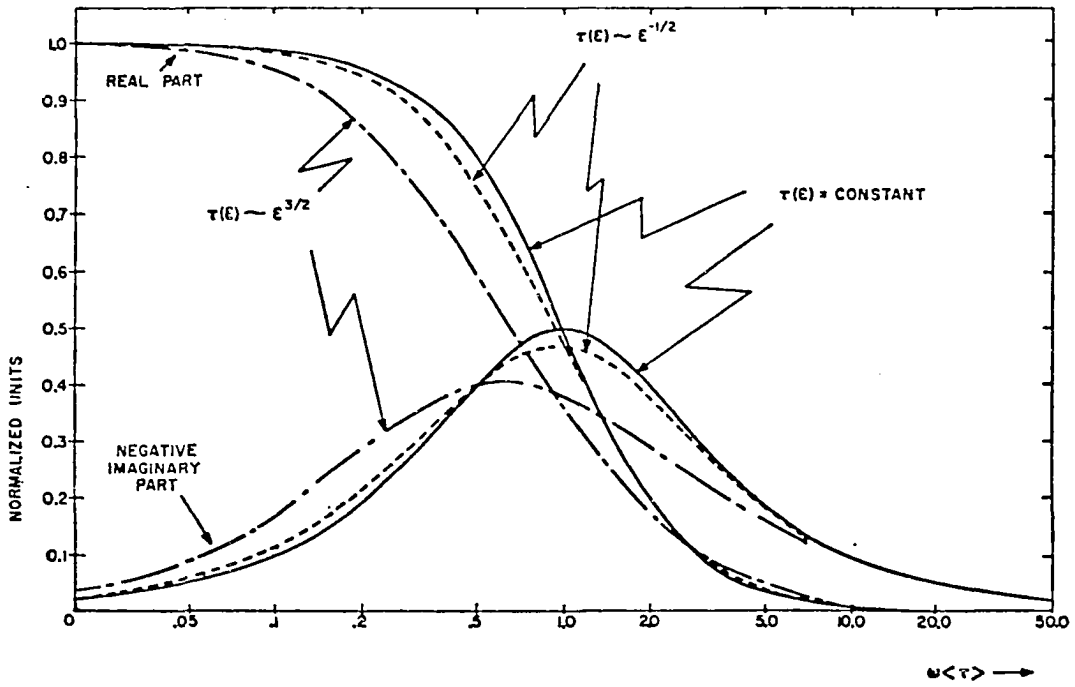

Fig. 9. Real and imaginary parts of $\frac{\sigma(\omega)}{\sigma(0)}$ for single-valley model and nondegenerate statistics (Reproduced from Champlin, Phys. Rev. 130, p. 1374. (1963))

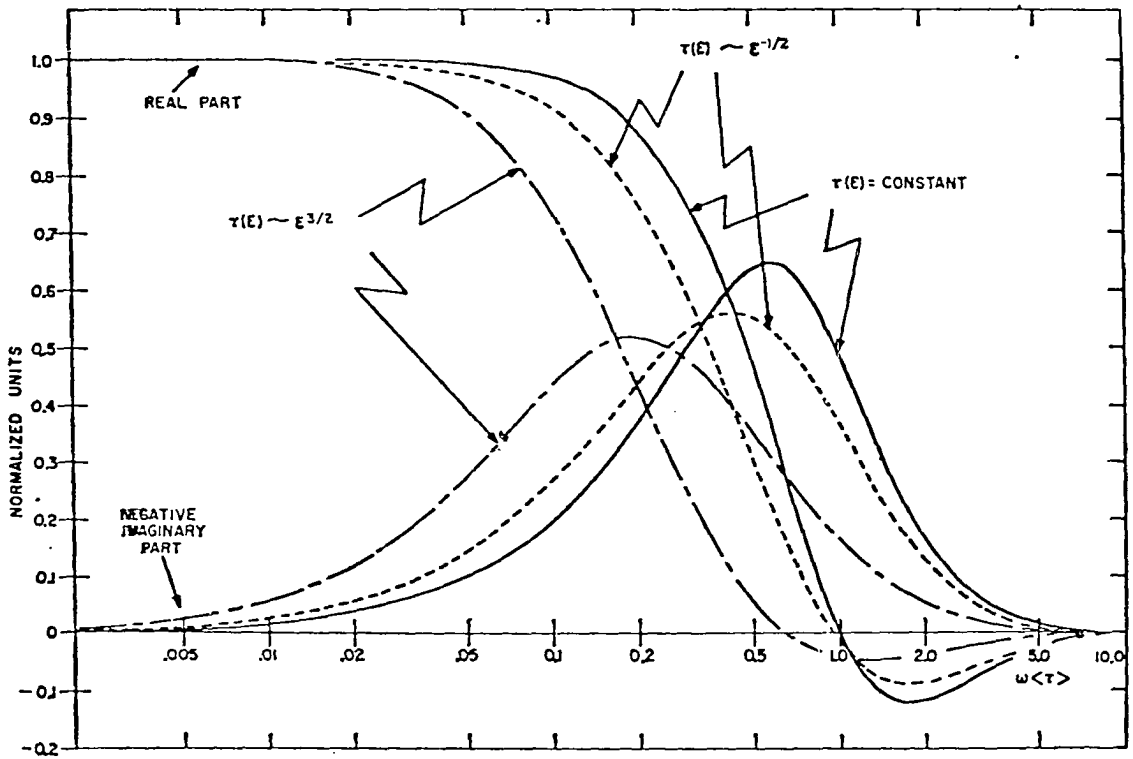

Fig. 10. Real and imaginary parts of $\frac{\theta(\omega)}{\theta(0)}$ for single-valley model and nondegenerate statistics
(reproduced from Champlin, Phys. Rev. 130, p. 1374, (1963))

By the definition of Hall mobility as defined by Watanabe (13) one can easily derive the ratio of high frequency Hall mobility to d.c. Hall mobility for the simple model as mentioned above. According to Watanabe the Hall mobility u_H is defined as

$$u_H = \frac{1}{B} \frac{|\sigma_1|}{\mathrm{Re}\ (\sigma_0)} \tag{4.5}$$

where σ_0 and σ_1 are the conductivity matrix elements defined in the following equation

$$\begin{pmatrix} j_x \\ j_y \end{pmatrix} = \begin{pmatrix} \sigma 0 & \sigma 1 \\ -\sigma 1 & \sigma 0 \end{pmatrix} \begin{pmatrix} E_x \\ E_y \end{pmatrix} \tag{4.6}$$

So, by comparing Equation 4.6 with Equations 1.2 and 1.6 we have

$$\frac{u_H(\omega)}{u_H(0)} = \frac{\left|\frac{\theta(\omega)}{\theta(0)}\right|}{\mathrm{Re}\ \frac{\sigma(\omega)}{\sigma(0)}} \tag{4.7}$$

Figure 11 is a plot of Equation 4.7 as a function of $\omega\langle\tau\rangle$ for $\tau \propto {}^{-1/2}$ and $\tau \propto {}^{3/2}$. Data given in Fig. 9 and 10 were used in the calculation. The results shown in Fig. 11 indicate that the high frequency Hall mobility corresponding to impurity scattering ($\tau \propto {}^{3/2}$) is smaller than that corresponding to phonon scattering ($\tau \propto {}^{-1/2}$).

Recently, Champlin et al. (53) measured the microwave conductivity of p-type germanium at 24 GHz and reported that the microwave conductivity was very close to d.c. conductivity at room temperature but dropped below the latter with decreasing temperatures and that the microwave conductivity was approximately one-half the d.c. value of liquid nitrogen

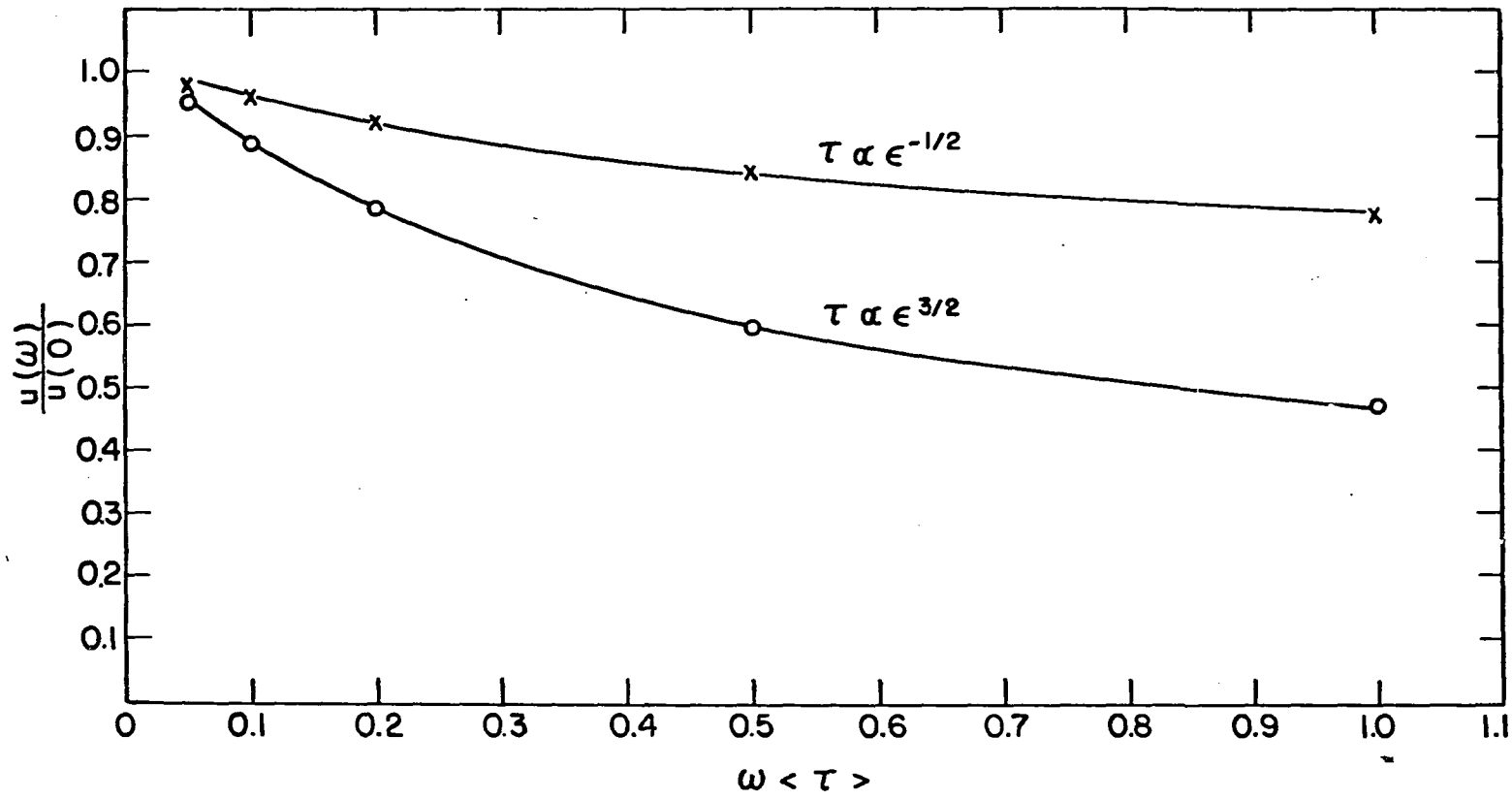

Fig. 11. $\frac{u_H(\omega)}{u_H(0)}$ for single-valley model and nondegenerate statistics

($\tau \propto \epsilon^{-1/2}$ represents phonon scattering and $\tau \propto \epsilon^{3/2}$ represents ionized impurity scattering)

temperature. The present results on Hall mobility showed that the per cent deviation between microwave and d.c. mobilities are 21%, 38%, and 45% at liquid nitrogen temperature for samples 439HGP, GP1, 439GP respectively, indicating a remarkable agreement with the conductivity results reported by Champlin.

B. Mixed Scattering by Lattice Vibrations and Ionized Impurities

In the standard treatment of mixed scattering, the force term (see Equation 1.1) in the Boltzmann equation is assumed to arise only from the effect of the applied fields and f is a function of velocity only so that $\frac{\partial f}{\partial r}$ vanishes. Also, relaxation time is estimated by defining an effective relaxation time τ_e by the relation (7)

$$\frac{1}{\tau_e} = \frac{1}{\tau_L} + \frac{1}{\tau_I} \tag{4.8}$$

where τ_L and τ_I are phonon and impurity scattering relaxation time respectively and are computed under the assumption that the two processes are independent. Also, this additive relationship is valid only if the effect of both impurity and phonon scattering can be represented by means of single relaxation time. In an actual case, however, a charge carrier may interact with a number of phonons while traversing the field of a single impurity center, and therefore the two processes cannot be strictly independent.

Reiss and Anderman (54) and Frisch and Lebowitz (55) have considered this problem and tried to avoid this inconsistency. They developed a more rigorous approach by treating the action of the impurities as part of the Hamiltonian of the system, but continuing to treat the effect of

phonon collisions by means of stochastic transition probabilities, i.e., the phonon scattering enters through the usual linear Boltzmann-type collision term and is described by the relaxation time τ. This treatment implies that the impurities are regarded as the source of an additional applied electric field with which the electrons are always interacting. Thus, one has to use a space-dependent, and velocity-dependent distribution function, and the problem of the independence of the two scattering processes does not exist. This approach introduces important changes in the problem, but does not appear to be easy to solve. Frisch and Lebowitz only showed that the addition of impurities always decreased the conductivity. By this general conclusion one would expect that, if a more rigorous approach were used in the analysis of the high frequency transport coefficients, the impurity scattering might further result in lower microwave Hall mobility as discussed in section VI, A.

C. Hole Contribution to the Dielectric Constant

The relative dielectric constant of germanium is usually assumed to be a constant 16. It arises from the polarization of lattice. At microwave frequencies, however, it becomes possible to observe the carrier contribution to the dielectric constant (56). The hole contribution to the dielectric constant can be expressed as (57)

$$D_{hole} = - \frac{Ne^2}{m\varepsilon_o} \left[\left(\frac{e}{m} \right)^2 \frac{1}{u_0 u_H} + \omega^2 \right], \qquad (4.9)$$

where D_{hole} = dielectric constant due to holes,

ε_o = dielectric constant of free space,

u_0 = d.c. mobility,

and u_H = Hall mobility.

This equation was derived on the assumption of a Maxwellian distribution of velocities for the holes, and an energy dependent relaxation time. Experimentally, Champlin et al. (35) reported that the inertia of the carrier could have a considerable influence on the dielectric constant of p-type germanium. Their results showed that the relative dielectric constant was 16 at room temperature but it dropped to about 3 at liquid nitrogen temperature. This difference is due to the hole contribution (negative) at $\omega\tau \gtrsim 1$.

To treat the impurity scattering Brooks (58) and Dingle (59) used a screened scattering potential

$$|V(r)| = \frac{e}{Dr} e^{-r/a}, \qquad (4.10)$$

where D = dielectric constant of the crystal,

and a = Debye-Hückel length (or screening distance).

This potential is inversely proportional to the dielectric constant. Thus, at high frequencies, the field of an impurity center ($\vec{E} = -\vec{\nabla}V$) which interacts with the charge carriers becomes stronger as the temperature decreases.

D. Conclusions

The present investigation has shown the following.

(1) The difference between the microwave and d.c. Hall mobility exists at low temperatures and the microwave Hall mobility is always lower than the corresponding d.c. value. The deviation becomes greater than 50% at

temperatures below liquid nitrogen.

(2) The impurity scattering may be responsible for the major part of the difference at low temperatures. The difference increases with increasing impurity concentration. With the same impurity concentration the scattering function may become stronger at low temperatures because of the modification of the scattering potential due to the negative contribution of holes to the dielectric constant at frequencies such that $\omega\tau \gtrsim 1$.

E. Future Work

Brooks (60) has pointed out that for p-type germanium, interband scattering is the principal mechanism that determines the relaxation time of the light holes, while intraband scattering is the principal mechanism that determine the relaxation time of the heavy holes. Thus, the scattering depends essentially on the density of final states which, in either case, is principally the density of states for the heavy hole band. Therefore, the collision frequencies of the two types of holes are approximately equal. The relaxation times, which are the reciprocals of the collision frequencies, must also be equal for two types of holes. Although this argument has not yet been proven, it seems to be a reasonable approximation. (In the cyclotron resonance measurement, the relaxation times of the light and heavy holes were estimated to be approximately equal on the basis of line width (20)). So, if we assume the relaxation times of the two kinds of holes to be equal, we can simplify the quantitative analysis by writing the ratio of the Hall

mobility at microwave frequencies to the Hall mobility at direct current. From Watanabe's formula (13),

$$u_H = \frac{e \Sigma \frac{n_i}{m_i^2}}{\Sigma \frac{n_i}{m_i}} \times \frac{\left| \left\langle \frac{\tau^2}{(1 + i\omega\tau)^2} \right\rangle \right|}{\mathrm{Re} \left\langle \frac{\tau}{1 + i\omega\tau} \right\rangle}$$

we have $$\frac{(u_H)_{mv}}{(u_H)_{dc}} = \frac{\langle \tau \rangle}{\langle \tau^2 \rangle} \frac{\left| \left\langle \frac{\tau^2}{(1 + i\omega\tau)^2} \right\rangle \right|}{\mathrm{Re} \left\langle \frac{\tau}{1 + i\omega\tau} \right\rangle}$$

This ratio is independent of effective mass and density of carriers. The quantity on the left hand side can be determined from the experimental results. The only unknown term is the relaxation time τ. With the present experimental results and with the assistance of a computer, it is therefore possible to calculate the temperature dependence of the relaxation time. The d.c. Hall mobility can then be used to obtain the temperature dependence of the conductivity effective mass.

V. LITERATURE CITED

1. Kittel, C. Elementary statistical physics. 1st ed. New York, N. Y., John Wiley & Sons, Inc. 1964.

2. Seitz, F. Note on the theory of resistance of cubic semiconductor in a magnetic field. Phys. Rev. 79: 372. 1950.

3. Davis, L., Jr. Change of resistance in a magnetic field. Phys. Rev. 56: 93. 1939.

4. Kittel, C. Introduction to solid state physics. 2nd ed. New York, N. Y., John Wiley & Sons, Inc. 1963.

5. Blatt, F. J. Theory of mobility of electrons in solids. In Seitz, F. and Turnbull, D., eds. Solid state physics. Vol. 4, pp. 199-366. New York, N. Y., Academic Press, Inc. 1957.

6. Donovan, B. The Hall effect in metals at high frequencies. Proc. Phys. Soc. Lond. A68: 1026. 1955.

7. Ziman, J. M. Electrons and phonons. 1st ed. Amen House, London, Britain, Clarendon Press. 1962.

8. Stephen, M. J. and Lidard, A. B. The Faraday effect in semiconductors. J. Phys. Chem. Solids 9: 43. 1959.

9. Mitchell, E. W. J. The infra-red Faraday effect due to free carriers in a semiconductor. Proc. Phys. Soc. Lond. B68: 973. 1955.

10. Nishina, Y. Microwave measurement of Hall mobilities in semiconductors. Unpublished Ph.D. thesis. Ames, Iowa, Library, Iowa State University of Science and Technology. 1961.

11. Ho, B. L. Microwave mobilities of holes in p-type germanium. Unpublished M.S. thesis. Ames, Iowa, Library, Iowa State University of Science and Technology. 1964.

12. Hambleton, G. E. and Gartner, W. W. Microwave Hall effect in germanium and silicon at 20 Gc/s. J. Phys. Chem. Solids 8: 329. 1959.

13. Watanabe, N. Hall effect in n- and p-type germanium at 24 Gc/s. J. Phys. Soc. Japan 16: 1979. 1961.

14. Herman, F. Theoretical investigation of the electronic energy band structure of solids. Rev. Modern Phys. 30: 102. 1958.

15. Kane, E. O. Energy band structure in p-type germanium and silicon. J. Phys. Chem. Solids 1: 82. 1956.

16. Barrie, R. Electronic conduction in solids with spherically symmetric band structure. Proc. Phys. Soc. London 69B: 553. 1956.

17. Dexter, R. N., Zeiger, H. J., and Lax, B. Anisotropy of cyclotron resonance of holes in germanium. Phys. Rev. 95: 557. 1954.

18. Lax, B., Zeiger, H. J., and Dexter, R. N. Anisotropy of cyclotron resonance in germanium. Physica 20: 818. 1954.

19. Dresselhaus, G., Kip, A. F., and Kittel, C. Spin-orbit interaction and the effective masses of holes in germanium. Phys. Rev. 95: 568. 1954.

20. Dresselhaus, G., Kip, A. F., and Kittel, C. Cyclotron resonance of electrons and holes in silicon and germanium crystals. Phys. Rev. 98: 368. 1955.

21. Willardson, R. K., Harman, T. C., and Beer, A. C. Transverse Hall and magnetoresistance effects in p-type germanium. Phys. Rev. 96: 1512. 1954.

22. Lawrence, R. The temperature dependence of drift mobility in germanium. Phys. Rev. 89: 1295. 1953.

23. Prince, M. B. Drift mobilities in semiconductors I. germanium. Phys. Rev. 92: 681. 1953.

24. Vinogradova, M. N., Golikova, O. A., Mitronin, B. P., and Stil'bans, L. S. The mechanism of carrier scattering in p-type germanium. Soviet Phys. Solid State 2: 1928. 1961.

25. Beer, A. C. and Willardson, R. K. Hall and transverse magneto-resistance effects for warped bands and mixed scattering. Phys. Rev. 110: 1286. 1958.

26. Tauber, G. E. Transport phenomena in germanium and silicon. J. Phys. Chem. Solids. 23: 7. 1962.

27. Bray, R. and Brown, D. M. Lattice scattering mechanism in p-type germanium. In Proc. intern. conf. on semiconductors Prague 1960. pp. 82-85. House Czech. Acad. Sci. Prague. 1961.

28. Brown, D. M. and Bray, R. Analysis of lattice and ionized impurity scattering in p-type germanium. Phys. Rev. 127: 1593. 1962.

29. Becker, J. H. Magnetic field dependence of the Hall coefficient and electrical conductivity in semiconductors. Bull. Am. Phys. Soc. II. 2: 57. 1957.

30. Willardson, R. K. and Beer, A. C. Effects of ionized impurity scattering on the magnetoresistance in Ge. Bull. Am. Phys. Soc. II. 2: 142. 1957.

31. Bagguley, D. M. S., Strandling, R. A., and Whiting, J. S. S. Cyclotron resonance over a wide temperature range. I. Germanium. Proc. Roy. Soc. A262: 340. 1961.

32. Bagguley, D. M. S. and Strandling, R. A. Cyclotron resonance at 4mm wavelength. Proc. Phys. Soc. Lond. 78: 1078. 1961.

33. Walton, A. K. and Moss, T. S. Free-carrier Faraday effect in n-type germanium. J. Appl. Phys. 30: 951. 1959.

34. Cardona, M., Paul, W., and Brooks, H. The temperature dependence of the polarizability of the free carriers in germanium and silicon. Helv. Phys. Acta. 33: 329. 1960.

35. Champlin, K. S., Armstrong, D. B., Holm, J. D., and Patrin, N. A. Temperature dependence of conductivity effective mass of holes in germanium. Phys. Rev. Letters. 14: 547. 1965.

36. Champlin, K. S., Armstrong, D. B., and Gunderson, P. D. Charge carrier inertia in semiconductors. Proc. I. E. E. E. 52: 677. 1965.

37. Harrison, W. A. Scattering of electrons by lattice vibration in nonpolar crystals. Phys. Rev. 104: 1281. 1956.

38. Bir, G. L. and Pikus, G. E. Theory of the deformation potential for semiconductors with a complex band structure. Soviet Phys. Solid State 2: 2039. 1961.

39. Ehrenreich, H. and Overhauser, A. W. Scattering of holes by phonon in germanium. Phys. Rev. 104: 331. 1956.

40. Ehrenreich, H. and Overhauser, A. W. Lattice-scattering mobility of holes in germanium. Phys. Rev. 104: 649. 1956.

41. Conwell, E. Lattice mobility of hot carriers. J. Phys. Chem. Solids 8: 234. 1959.

42. Appel, J. and Bray, R. Effect of hole-hole scattering on the mobility of p-type germanium. Phys. Rev. 127: 1603. 1962.

43. Nishina, Y. and Danielson, G. C. Microwave measurement of Hall mobility: experimental method. Rev. Sci. Inst. 32: 790. 1961.

44. Liu, S. H., Nishina, Y., and Good, R. H., Jr. Microwave measurement of Hall mobility: analysis of apparatus. Rev. Sci. Inst. 32: 784. 1961.

45. Finnemore, D. K., Osterson, J. E., and Stromberg, T. F. U.S. Atomic Energy Commission Report IS-1046. (Iowa State University of Science and Technology, Ames, Iowa, Inst. for Atomic Research) 1964.

46. Powell, R. L., Bunch, M. D., and Corruccini, R. J. Low temperature thermocouples. I. Gold-cobalt or constantant versus copper or "normal" silver. Cryogenics 1: 139. 1961.

47. Zrudsky, D. R. Hall coefficient and resistivity of a MgSi single crystal from 4°K to 300°K. Unpublished M.S. thesis. Ames, Iowa, Library, Iowa State University of Science and Technology. 1959.

48. Heller, M. W. Seeback effect in magnesium silicide. Unpublished Ph.D. thesis. Ames, Iowa, Library, Iowa State University of Science and Technology. 1960.

49. Champlin, K. S. Frequency dependence of high-frequency transport properties of cubic crystals. Phys. Rev. 130: 1374. 1963.

50. Erginsoy, C. Neutral impurity scattering in semiconductors. Phys. Rev. 79: 1013. 1950.

51. Shockley, W. and Bardeen, J. Energy bands and mobilities in monatomic semiconductors. Phys. Rev. 77: 407. 1949.

52. Conwell, E. M. and Weisskopf, V. F. Theory of impurity scattering in semiconductors. Phys. Rev. 77: 388. 1950.

53. Champlin, K. S., Armstrong, D. B., and Gunderson, P. D. Charge carrier inertia in semiconductors. I. E. E. E. 52: 677. 1964.

54. Reiss, H. and Anderman, A. I. Scattering of electrons by phonons and impurities in semiconductors. Phys. Rev. 122: 1135. 1961.

55. Frisch, H. L. and Lebowitz, J. L. Electron transport at high temperatures in the presence of impurities. Phys. Rev. 123: 1542. 1961.

56. Shockley, W. and Benedict, T. S. Microwave observation of the collision frequency of electrons in germanium. Phys. Rev. 89: 1152. 1953.

57. Benedict, T. S. Microwave observation of the collision frequency of holes in germanium. Phys. Rev. 91: 1565. 1953.

58. Brooks, H. Scattering by ionized impurities in semiconductors. Phys. Rev. 83: 879. 1951.

59. Dingle, R. B. Scattering of electrons and holes by charged donors and acceptors in semiconductors. Phil. Mag. 46: 831. 1955.

60. Brooks, H. Theory of the electrical properties of germanium and silicon. In Marton, L. ed. Advances in electronic and electron physics. Vol. 2. pp. 85-182. New York, N. Y., Academic Press, Inc. 1955.

VI. ACKNOWLEDGMENTS

The author wishes to express his gratitude to his major professor in electrical engineering, Dr. A. V. Pohm, for his very kind guidance and generous support which made the continuation of this research and graduate study possible.

Special gratitude is extended to Dr. G. C. Danielson, in whose laboratory this research was conducted, for his continuous understanding, technical guidance, encouragement and full support during the whole period of the author's research and graduate studies at Iowa State University.

Mr. P. H. Sidle's help in designing the low temperature cryostat and Mr. O. M. Sevde's help in building the cryostat and vacuum system are acknowledged and highly appreciated.

Appreciation is also extended to the Institute for Atomic Research at Iowa State University for the financial support which made this investigation possible.

VII. APPENDIX

Table 1. d.c. electrical measurement of p-type germanium (439HGP)

Temperature (°K)	Hall coefficient R_h (m^3/coulomb) (x 10^{-3})	Resistivity ρ (ohm-m) (x 10^{-2})	Hall mobility u_H (m^2/V-sec)
4.8	7172.0	322.0	2.23
5.9	7051.0	289.0	2.44
7.0	582.0	22.50	2.58
11.5	489.0	18.30	2.67
14.1	134.0	5.320	2.51
16.0	71.2	2.860	2.49
20.0	27.7	1.140	2.42
25.0	13.9	0.584	2.37
32.0	8.64	0.376	2.30
39.0	7.24	0.327	2.21
46.0	6.66	0.318	2.10
53.0	6.35	0.322	1.97
60.0	6.05	0.334	1.81
65.0	6.13	0.360	1.70
70.0	5.73	0.372	1.54
74.2	6.06	0.401	1.51
81.0	6.21	0.448	1.39
87.0	6.00	0.464	1.29
94.0	6.03	0.509	1.19
102.0	6.21	0.580	1.02
110.0	6.58	0.652	1.01
118.0	6.76	0.724	0.933
125.0	7.26	0.823	0.882
133.3	7.47	0.931	0.801
140.0	7.82	1.020	0.767

Table 1. (Continued)

Temperature (°K)	Hall coefficient R_h (m^3/coulomb) (x 10^{-3})	Resistivity (ohm-m) (x 10^{-2})	Hall mobility u_H (m^2/V-sec)
145.2	8.02	1.084	0.740
155.2	8.08	1.221	0.662
165.0	8.45	1.342	0.630
177.0	9.32	1.641	0.568
189.6	10.27	1.963	0.523
200.0	9.71	2.031	0.478
210.0	9.76	2.147	0.449
220.3	10.55	2.493	0.423
230.5	10.82	2.711	0.399
242.3	10.66	2.874	0.371
258.0	11.93	3.480	0.343
269.4	11.98	3.722	0.322
272.0	12.41	3.916	0.317
277.0	12.54	4.044	0.310
281.0	12.91	4.273	0.302
288.0	12.77	4.347	0.292
294.0	12.89	4.509	0.286
300.0	14.60	5.336	0.274

Table 2. d.c. electrical measurement of p-type germanium (GP1)

Temperature (°K)	Hall coefficient R_h (m^3/coulomb) (x 10^{-3})	Resistivity ρ (ohm-m) (x 10^{-2})	Hall mobility u_H (m^2/V-sec)
4.8	51.45	5.92	0.869
7.2	55.45	5.90	0.940
10.0	47.70	4.68	1.020
15.2	22.14	1.96	1.129
18.3	12.30	1.05	1.168
20.0	6.876	0.582	1.180
23.8	4.436	0.374	1.184
28.0	3.045	0.260	1.172
31.8	2.474	0.208	1.185
34.5	2.158	0.181	1.190
39.5	1.797	0.150	1.191
46.6	1.506	0.127	1.186
57.8	1.276	0.112	1.144
64.0	1.205	0.109	1.109
66.7	1.179	0.108	1.088
69.3	1.158	0.108	1.069
73.8	1.129	0.109	1.035
75.9	1.118	0.110	1.020
79.7	1.103	0.111	0.992
84.3	1.086	0.114	0.952
91.4	1.069	0.119	0.898
102.6	1.058	0.131	0.807
111.9	1.056	0.142	0.745
106.0	1.055	0.137	0.769
113.5	1.054	0.144	0.733
117.4	1.056	0.149	0.709
122.5	1.055	0.156	0.675
129.7	1.059	0.167	0.634
143.0	1.071	0.190	0.565
153.0	1.081	0.210	0.515
155.3	1.094	0.216	0.508
162.3	1.104	0.232	0.476
167.5	1.105	0.244	0.453
169.8	1.108	0.250	0.443
172.3	1.115	0.257	0.434

Table 2. (Continued)

Temperature (°K)	Hall coefficient R_h (m^3/coulomb) (x 10^{-3})	Resistivity ρ (ohm-m) (x 10^{-2})	Hall mobility u_H (m^2/V-sec)
174.0	1.120	0.261	0.430
174.7	1.157	0.263	0.440
179.5	1.197	0.274	0.437
201.0	1.195	0.329	0.364
217.8	1.216	0.377	0.323
227.8	1.215	0.408	0.298
270.7	1.206	0.573	0.210
242.3	1.181	0.463	0.255
258.0	1.198	0.523	0.229
280.0	1.210	0.743	0.198
291.8	1.206	0.663	0.182
299.0	1.221	0.700	0.174

Table 3. d.c. electrical measurement of p-type germanium (439GP)

Temperature (°K)	Hall coefficient R_h (m^3/coulomb) (x 10^{-3})	Resistivity ρ (ohm-m) (x 10^{-2})	Hall mobility u_H (m^2/V-sec)
5.5	88.80	1.930	0.460
9.5	68.54	1.221	0.562
14.0	46.74	0.740	0.617
19.0	31.14	0.475	0.654
25.0	19.44	0.279	0.698
28.4	15.96	0.222	0.718
32.0	13.52	0.185	0.734
34.2	12.52	0.166	0.754
37.0	10.73	0.141	0.757
39.0	9.88	0.132	0.748

Table 3. (Continued)

Temperature (°K)	Hall coefficient R_h (m^3/coulomb) (x 10^{-3})	Resistivity ρ (ohm-m) (x 10^{-2})	Hall mobility u_H (m^2/V-sec)
42.0	9.00	0.118	0.763
48.0	7.68	0.101	0.762
49.7	7.51	0.0971	0.774
52.0	7.04	0.0929	0.757
54.2	6.68	0.0887	0.753
58.0	6.37	0.0855	0.746
63.0	5.89	0.0814	0.724
68.0	5.66	0.0784	0.722
72.0	5.41	0.0778	0.696
79.1	5.31	0.0773	0.687
87.0	5.23	0.0779	0.671
94.0	5.02	0.0794	0.632
99.3	4.90	0.0813	0.603
113.0	4.77	0.0866	0.551
118.0	4.77	0.0903	0.528
127.0	4.93	0.0969	0.509
141.4	5.14	0.110	0.409
150.4	5.11	0.118	0.432
159.6	5.23	0.129	0.407
170.0	5.34	0.141	0.379
182.0	5.44	0.156	0.348
189.5	5.54	0.167	0.332
198.0	5.64	0.180	0.313
208.0	5.83	0.197	0.296
219.0	5.92	0.216	0.274
258.4	6.12	0.290	0.211
271.0	6.06	0.317	0.191
286.0	6.18	0.351	0.176
300.0	6.33	0.391	0.162

Table 4. Magnetic field dependence of $\sqrt{\frac{P_2}{P_1}}$ for p-type germanium single crystals

Magnetic field B (Wb/m^2)	$\sqrt{\frac{P_2}{P_1}}$ (x 10^{-3})	$\sqrt{\frac{P_2}{P_1}}$ (x 10^{-3})	$\sqrt{\frac{P_2}{P_2}}$ (x 10^{-3})
	A. Sample 439HGP		
	Temp. 300°K	Temp. 78°K	Temp. 5.5°K
0.17	2.09	5.750	7.372
0.20	2.45	6.781	8.640
0.28	3.41	9.433	11.58
0.36	4.42	11.91	13.46
0.46	5.41	14.20	15.01
0.57	6.49	16.76	16.00
0.69	7.34	18.64	16.36
0.82	7.96	19.59	16.64
	B. Sample GP1		
	Temp. 300°K	Temp. 78°K	Temp. 6°K
0.17	2.26	6.160	9.262
0.20	2.68	7.234	10.85
0.28	3.77	10.07	14.11
0.36	4.81	12.74	16.24
0.46	5.94	15.58	17.89
0.57	7.31	18.26	19.04
0.69	8.33	20.17	19.76
0.82	9.24	21.73	20.22
	C. Sample 439GP		
	Temp. 300°K	Temp. 77.8°K	Temp. 5.3°K
0.17	1.15	6.363	7.652
0.20	1.35	7.410	8.943
0.28	1.93	10.44	12.45
0.36	2.45	13.15	15.07
0.46	3.04	16.11	17.26
0.57	3.62	18.70	18.94
0.69	4.11	21.12	19.97
0.82	4.50	22.69	20.66

Table 5. Microwave Hall mobility of p-type germanium (439HGP) at low temperature

Temperature (°K)	2α ($\times 10^{-3}$)	$\frac{Y_o + G + 2\alpha}{2\alpha}$	$\sqrt{\frac{P_2}{P_1}}\,\frac{2}{\lvert 1 + R \rvert B_o}$ ($\times 10^{-3}$)	Hall mobility u_H (m^2/sec-V)
5.5	1.594	5.175	2.552	1.32
7.5	1.350	5.804	2.533	1.47
9.6	1.135	6.608	2.239	1.48
14.3	0.8392	8.561	1.740	1.49
19.4	0.5727	11.82	1.294	1.53
20.0	0.5332	11.99	1.268	1.52
27.0	0.3939	15.23	0.9718	1.48
34.0	0.3638	15.68	0.8928	1.40
40.2	0.3534	15.14	0.9380	1.42
47.8	0.3475	14.49	0.9177	1.33
54.0	0.3514	13.48	1.001	1.35
60.0	0.3575	12.15	1.029	1.25
70.0	0.3749	10.95	1.032	1.13
78.0	0.3939	10.72	1.026	1.10
86.0	0.4179	10.75	0.9672	1.04
96.2	0.4515	9.793	1.003	0.982
105.8	0.4832	9.436	0.9569	0.903
116.0	0.5242	8.925	0.9198	0.821
126.0	0.5674	8.489	0.9402	0.798
136.2	0.6064	8.105	0.9046	0.733
146.0	0.6476	7.803	0.8485	0.662
156.0	0.6918	7.475	0.8576	0.641
166.0	0.7337	7.212	0.8359	0.603
176.0	0.7751	6.968	0.8111	0.565
186.0	0.8381	6.618	0.8161	0.540
196.0	0.8836	6.412	0.7702	0.494
206.0	0.9301	6.196	0.7281	0.451
216.0	0.9944	5.895	0.7413	0.437
226.0	1.038	5.763	0.7128	0.412
236.0	1.091	5.572	0.6998	0.390
246.0	1.127	5.484	0.6711	0.368
256.0	1.189	5.262	0.6632	0.349
270.0	1.294	4.914	0.6533	0.321
285.0	1.351	4.777	0.6217	0.297
300.0	1.381	4.744	0.5755	0.273

Table 6. Microwave Hall mobility of p-type germanium (GP1) at low temperature

Temperature (°K)	2α ($\times 10^{-3}$)	$\frac{Y_o + G + 2\alpha}{2\alpha}$	$\sqrt{\frac{P_2}{P_1}}\ \frac{2}{\lvert 1 + R \rvert\ B_o}$ ($\times 10^{-3}$)	Hall mobility u_H (m^2/sec-V)
6	6.84	1.106	29.40	0.325
8	5.56	1.315	30.50	0.401
10	5.22	1.364	31.55	0.430
12	4.55	1.502	30.61	0.460
16	3.53	1.870	28.34	0.530
19	2.60	2.448	22.96	0.562
27	1.38	4.451	13.48	0.600
30	1.25	4.683	13.67	0.640
34	1.14	4.950	12.73	0.630
38	1.04	5.167	12.00	0.620
44	0.957	5.369	11.74	0.630
55	0.886	5.527	11.49	0.635
65	0.858	5.455	11.00	0.600
75	0.864	5.182	11.60	0.601
78	0.867	5.127	11.53	0.591
84	0.888	5.108	11.47	0.585
95	0.912	5.080	11.28	0.573
105	0.953	4.870	11.13	0.542
116	0.992	4.472	11.13	0.531
125	1.04	4.667	8.843	0.501
135	1.09	4.529	10.42	0.472
144	1.14	4.434	10.38	0.460
155	1.20	4.358	10.10	0.440
165	1.26	4.247	9.537	0.405
176	1.33	4.083	9.431	0.385
185	1.39	3.986	9.284	0.370
194	1.46	3.858	9.289	0.358
205	1.52	3.760	8.778	0.330
214	1.59	3.656	8.563	0.313
225	1.66	3.550	8.143	0.289
236	1.73	3.467	7.874	0.273
244	1.80	3.379	7.549	0.255
255	1.86	3.300	7.394	0.244
265	1.93	3.224	6.857	0.221
275	2.01	3.127	6.622	0.207
285	2.09	3.033	6.366	0.193
300	2.18	2.907	6.088	0.177

Table 7. Microwave Hall mobility of p-type germanium (439GP) at low temperature

Temperature (°K)	2α ($\times 10^{-3}$)	$\frac{Y_o + G + 2\alpha}{2\alpha}$	$\sqrt{\frac{P_2}{P_1}}\,\frac{2}{\lvert 1 + R\rvert B_o}$ ($\times 10^{-3}$)	Hall mobility u_H (m^2/sec-V)
5.3	2.209	1.247	8.821	0.110
5.7	2.209	1.223	9.485	0.116
8.5	1.894	1.407	11.09	0.156
9.7	1.765	1.482	10.68	0.169
13.9	1.398	1.843	11.29	0.208
15.4	1.283	1.977	11.33	0.224
19.0	1.084	2.304	10.98	0.253
23.0	0.9105	2.711	9.889	0.268
27.0	0.7921	3.078	9.421	0.290
32.0	0.6869	3.520	9.120	0.321
36.0	0.6204	3.881	8.220	0.319
41.0	0.5632	4.276	7.928	0.339
46.0	0.5238	4.635	7.400	0.343
52.0	0.4902	4.933	7.338	0.362
59.0	0.4665	5.205	7.012	0.365
66.0	0.4526	5.409	6.637	0.359
71.0	0.4484	5.524	6.698	0.370
77.8	0.4468	5.637	6.688	0.377
84.0	0.4477	5.667	6.511	0.369
90.0	0.4502	5.700	6.737	0.384
100.0	0.4577	5.694	6.358	0.362
110.0	0.4692	5.637	6.582	0.371
119.0	0.4843	5.565	6.613	0.368
130.0	0.5066	5.436	6.806	0.370
137.0	0.5211	5.519	6.541	0.361
146.0	0.5427	5.401	6.518	0.352
155.0	0.5654	5.394	6.378	0.344
166.0	0.5927	5.379	6.098	0.328
178.0	0.6240	5.362	5.986	0.321
186.0	0.6473	5.444	5.694	0.310
197.0	0.6802	5.470	5.429	0.297
209.0	0.7175	5.448	5.195	0.283
220.0	0.7504	5.498	4.875	0.268
231.0	0.7829	5.573	4.561	0.254
240.0	0.8477	5.403	4.442	0.240
250.0	0.8406	5.719	3.953	0.226
260.0	0.8720	5.784	3.649	0.211
274.0	0.9162	5.774	3.377	0.195
286.0	0.9560	5.813	3.097	0.180
300.0	1.005	5.765	2.810	0.1621

Table 8. $\frac{(u_H)_{dc} - (u_H)_{mv}}{(u_H)_{dc}}$ vs. temperature

Temperature (°K)	$\frac{(u_H)_{dc} - (u_H)_{mv}}{(u_H)_{dc}}$		
	Sample 439HGP	Sample GP1	Sample 439GP
6	44.6	64.7	74.6
10	43.1	58.3	71.2
15	41.2	53.6	66.5
20	39.5	51.3	64.1
30	37.0	49.2	60.4
40	34.4	48.4	58.2
50	31.3	47.0	54.8
60	28.0	44.2	51.4
70	24.4	41.5	48.5
80	21.4	38.1	44.5
100	15.2	31.5	37.8
150	7.0	15.4	21.2
200	0	7.4	8.3